Atmospheric Research 185 (2017) 142–157

Contents lists available at ScienceDirect

Atmospheric Research

journal homepage: www.elsevier.com/locate/atmosres

Characteristics of the global thermal tropopause derived from multiple radio occultation measurements

Wei Li [a,*], Yun-bin Yuan [a], Yan-Ju Chai [a], Yuei-An Liou [b,c,*], Ji-kun Ou [a], Shi-ming Zhong [a]

[a] State Key Laboratory of Geodesy and Earth's Dynamics, Institute of Geodesy and Geophysics, Chinese Academy of Sciences, 340 XuDong Rd., Wuhan, Hubei Province, China
[b] Center for Space and Remote Sensing Research (CSRSR), National Central University, Chungli District, Taoyuan City, Taiwan
[c] Taiwan GIS Center (TGIC), Taipei, Taiwan

ARTICLE INFO

Article history:
Received 26 May 2015
Received in revised form 30 May 2016
Accepted 20 September 2016
Available online 21 September 2016

Keywords:
Global tropopause
Annual cycle
Interannual variation
Diurnal variation
Radio occultation
FORMOSAT-3/COSMIC

ABSTRACT

Thermal tropopause represents the region of the atmosphere where the environmental lapse rate changes from tropospheric positive to stratospheric negative. It also defines the altitude of the atmosphere beneath which significant weather perturbations occur except occasional overshooting thunderstorms in the tropical regions. Accordingly, how the temporal and spatial variability of thermal tropopause behaves is of great concern in atmospheric research and, hence, investigated in this study by using radio occultation (RO) observations obtained from seven space missions during the period from May 2001 to April 2013 (with a total of 6,075,359 occultations). While RO observations have been demonstrated to provide precise measurements of temperature profiles of the atmosphere, their results are inter-compared before further use in our analysis, showing expected high-precision observations with mean differences < 0.06 K and standard deviations < 1.6 K in the upper troposphere and lower stratosphere. Given a rather large data set of multi- space-mission RO measurements taken globally, a very detailed description of spatial structure and variability of the tropopause is revealed, and monthly mean zonal mean tropopause parameters in each 2° latitude band from 90°S to 90°N can be obtained. Many interesting features of seasonal cycle, spatial distribution, interannual variation, and diurnal variation of the thermal tropopause are observed. For examples, except for the primary minimum in January, the equatorial tropopause temperature exhibits a secondary minimum in April, possibly caused by the strongly combined wave forcing from two hemispheres; During the boreal winter over the tropics, the distribution of tropopause temperature extrema do not totally coincide with the altitude extrema spatially, and the former has a better agreement with the locations of strong tropical convection systems; Notable zonal asymmetries in interannual characteristics are observed in both tropical and extratropical regions. In both the tropics and Arctic, close correlation of the interannual variations is revealed between tropopause parameters and stratospheric temperatures in localized regions as well as zonal mean results while no such relationship is observed in the middle latitudes; and Diurnal variation of the equatorial tropopause shows warmer temperature in the morning and cooler value at midnight.

1. Introduction

The tropopause region, which separates the turbulent mixing-dominated troposphere from the more stably stratified stratosphere, is an important part of the earth's atmospheric system. The tropopause has recently received increasing attention because it is considered to be a useful indicator for the long-term climate change (Santer et al., 2003a; Santer et al., 2003b; Sausen and Santer, 2003). A robust increase in tropopause height (decrease in tropopause pressure and temperature) during the last few decades has been discovered either in the tropics (Seidel et al., 2001) or on a global scale (Santer et al., 2003a; Seidel and Randel, 2006). The simulation study of Santer et al. (2003a) indicated that changes in tropopause parameters should be largely attributed to anthropogenic forcing. The climatology of tropopause is also crucial for the mass and energy exchange between the stratosphere and troposphere (Holton et al., 1995; Shepherd, 2002). Characteristics of the temporal and spatial structures of the tropopause parameters have been presented primarily for the tropical tropopause (Reid and Gage, 1996; Highwood and Hoskins, 1998; Seidel et al., 2001; Gettelman and Forster, 2002), while comparatively less work has been done for the polar tropopause (Highwood et al., 2000; Zängl and Hoinka, 2001). Hoinka (1998, 1999) gave a comprehensive description of global tropopause through combining the thermal (lapse-rate) with the dynamical (potential vorticity) definition of tropopause. Those climatological studies of tropopause relied mainly on radiosonde or weather reanalysis data. However, these two data sources also have obvious drawbacks, since the weather reanalysis data usually suffer from

* Corresponding authors.
E-mail addresses: liwei@whigg.ac.cn (W. Li), yueian@csrsr.ncu.edu.tw (Y.-A. Liou).

http://dx.doi.org/10.1016/j.atmosres.2016.09.013
0169-8095/

coarse vertical resolution and radiosonde observations are sparse in the ocean and polar regions.

Recently, GPS (global positioning system) RO, which provides accurate pressure, temperature, and humidity measurements, has become a promising tool for atmospheric remote sensing (Liou et al., 2010). It is characterized by high vertical resolution, nearly uniform global sampling and long-term stability. Thus, RO temperature observations are ideally suitable for continuous identification and monitoring of the global tropopause. Initially, the thermal structure and temporal variability of the tropical tropopause were depicted by Nishida et al. (2000) and Randel et al. (2003) based on observations from GPS/MET (GPS/Meteorology), the first proof-of-concept GPS RO experiment. Then, Schmidt et al. (2004) extended their study by using a longer period of RO data from CHAMP (Challenging Minisatellite Payload). Climatological characteristics of the global tropopause were analyzed by Schmidt et al. (2005) and Kishore et al. (2006) using CHAMP and SAC-C (Satelite de Aplicaciones Cientificas-C) RO data simultaneously, while finer spatiotemporal structures are presented by Liou et al. (2010) and Son et al. (2011) using high spatial coverage RO data of FORMOSAT-3/COSMIC (Formosat Satellite-3 and Constellation Observing System for Meteorology, Ionosphere and Climate). Kumar et al. (2014) have investigated the impact of quasi-biennial oscillation (QBO) on the interannual variability of the cold point tropopause in the tropics using FORMOSAT-3/COSMIC RO data. The application of RO atmospheric profiles in long-term climate trend research was initially discussed by Foelsche et al. (2008) and Schmidt et al. (2008a), and Schmidt et al. (2008a) found a global increase of 4–7 m per year in tropopause height for the period May 2001–December 2007. In addition, Kuleshov et al. (2016) detected strong cooling in the lower stratosphere and warming in the upper troposphere for the period 2001–2008 over Antarctic, from both CHAMP RO observations and radiosonde data. In general, the tropopause parameters derived from RO soundings exhibit consistent characteristics with those from weather reanalysis or radiosonde data.

Due to the great usefulness of RO observations in operational numerical weather prediction, atmospheric structure sensing, and climate change detecting, more and more scientific research satellites are equipped with RO receiver currently, and if summed together, they are capable of providing thousands of operational soundings per day, more than the amount of global radiosonde profiles. In addition, the obvious tropopause influence on RO curves has been revealed by demonstrating sharp decreasing and next increasing of the amplitude signal amplitude with complex vertical structure of the refractivity in the troposphere (Liou et al., 2010). This study intends to conduct a comprehensive climatological study on the global tropopause from atmospheric measurements of multiple RO missions, which provide obviously higher spatiotemporal resolution than one single mission. Here, we employ data from seven missions: CHAMP, SAC-C, FORMOSAT-3/COSMIC, GRACE (Gravity Recovery and Climate Experiment), METOP/GRAS (Meteorological Operational Satellite Programme/GNSS (Global Navigation Satellite System) Receiver for Atmospheric Sounding), TerraSAR-X, and C/NOFS (Communications/Navigation Outage Forecasting System). The combination of these RO data covers the period between May 2001 and April 2013 and includes 6,075,359 atmospheric soundings. Such a large atmospheric data set derived from multiple RO missions enables description of more detailed structure and variability of the tropopause. A general structure of the tropopause is not the primary goal of present study since it has been extensively discussed before. We attempt to focus on the tropopause features that are less explored in earlier studies, such as the fine structure of seasonal cycle, interannual variation at different longitudes, diurnal variation, and so on.

This paper is organized as follows. Section 2 describes the RO data used in the study and the algorithms for identifying tropopause. In Section 3, an intercomparison of temperatures from different RO missions is conducted. Section 4 analyzes the climatology of global tropopause, including the seasonal cycle, spatial distribution, interannual variation, and diurnal variation. Finally, the summary of this study is given in Section 5.

2. Data and methods

An overview of the seven RO missions used in our study is shown in Table 1, in which information about their launch times, current statuses and the mission agencies are presented. In Table 1, each individual mission is assigned a short label and it will appear in the figures and tables of this paper instead of the original long mission name. Since only occultations from METOP-A satellite are used in this study, METOP/GRAS is labeled as METOPA.

The CHAMP measurements have generated the first long-term GPS RO data set (for about 8 years), and they also contributed to the preparation of several subsequent satellite missions with GPS RO capability (Wickert et al., 2001, 2004a, 2004b; Liou et al., 2005; Liou and Pavelyev, 2006; Schmidt et al., 2008a), e.g., SAC-C, GRACE, and FORMOSAT-3/COSMIC. The SAC-C mission was the first to implement and test the open-loop signal tracking on board and dramatically enhanced the RO sensing quality in the lower troposphere (Sokolovskiy et al., 2006). The RO measurements aboard GRACE were activated several years after the launch of the twin GRACE satellites, and they were based on the same type of BlackJack RO receiver as CHAMP and SAC-C (Wickert et al., 2005). The FORMOSAT-3/COSMIC mission incorporates six spacecraft, and provides typically ~1800 soundings per day, about an order of magnitude higher than the CHAMP, SAC-C, and GRACE missions (Liou et al., 2007; Fong et al., 2008a, 2008b, 2009; Anthes et al., 2008). The METOP/GRAS mission employed a new generation of instruments, which can perform both close-loop and raw-sampling modes (also known as open-loop) with frequencies at 50 Hz and 1000 Hz, respectively (von Engeln et al., 2008). The TerraSAR-X satellite is part of a twin-satellite project (TerraSAR-X/TanDEM-X), and equipped with an integrated GPS and occultation receiver (Wickert et al., 2008). More details on these RO missions are available from other references (Hajj et al., 2002, 2004; Schreiner et al., 2007, 2011; Wickert et al., 2009a, 2009b; von Engeln et al., 2011).

The COSMIC Data Analysis and Archive Center (CDAAC) processes raw RO measurements into atmospheric profiles and distributes RO products from level 0 to level 3 both in near real time and a few months after real time (Schreiner et al., 2003). It also provides re-processed data products 1–2 years later with highest quality in both accuracy and consistency, which significantly benefits climate researches. In this study, the level–2 wetPrf data of all the seven RO missions produced by the CDAAC are downloaded and used to investigate the tropopause characteristics.

The wetPrf data are generated through one-dimensional variational analysis using ECMWF (European Center for Medium-Range Weather Forecasts) low resolution analysis data and include atmospheric

Table 1
Overview of the seven RO missions used in this study.

Mission	Agency	Launch time	Status	Label
CHAMP	DLR	Jul. 2000	Completed	CHAMP
SAC-C	CONAE	Nov. 2000	Operational	SACC
FORMOSAT-3/COSMIC	NSPO, NOAA, UCAR	Apr. 2006	Operational	COSMIC
GRACE	NASA, DLR	Mar. 2002	Operational	GRACE
METOP/GRAS	EUMETSAT, ESA	Oct. 2006	Operational	METOPA
TerraSAR-X	DLR	Jun. 2007	Operational	TSX
C/NOFS	USAF STP	Apr. 2008	Operational	CNOFS

DLR: German Aerospace Center; CONAE: Comisión Nacional de Actividades Espaciales (Argentina); NSPO: National Space Program Office (Taiwan); NOAA: National Oceanic and Atmospheric Administration (U.S.); UCAR: University Corporation for Atmospheric Research (U.S.); NASA: National Aeronautics and Space Administration (U.S.); EUMETSAT: European Organization for the Exploitation of Meteorological Satellites; ESA: European Space Agency; USAF STP: United States Air Force Space Test Program.

Table 2
RO wetPrf data periods, versions, total numbers of profiles, and numbers of profiles per day used in this study. All data were downloaded from CDAAC.

Mission	Period (year/month)	Total number of profiles	Daily profiles	Data version
CHAMP	2001/5–2008/9	399,553	153	2009.2650
SAC-C	2001/8–2002/11	403,827	187	2007.3200
	2006/3–2011/8			2010.2640
FORMOSAT-3/COSMIC	2006/7–2013/4	3,701,309	1494	2010.2640
GRACE	2007/2–2013/2	251,964	127	2010.2640
METOP/GRAS	2007/9–2013/4	992,575	523	2011.2980
TerraSAR-X	2008/2–2012/10	264,162	190	2010.2640
C/NOFS	2010/3–2011/12	61,969	132	2010.2640

pressure, temperature, and water vapor pressure retrievals covering a height range from near the Earth's surface up to 40 km. All profiles are interpolated at 0.1 km vertical levels. Table 2 presents information on the wetPrf data periods, versions, total numbers of profiles, and numbers of daily profiles for the seven RO missions used in this study. Although the data versions exhibit minor differences, the products are still considered consistent because they are processed with similar algorithms. Note that, for FORMOSAT-3/COSMIC, the average number of daily observations is 1494, apparently lower than its designed number (1800 per day). This is because the observations of FORMOSAT-3/COSMIC had been degraded to approximately 1000 profiles per day from middle 2010 to middle 2012 due to a power problem, while the daily number results shown in Table 2 represent long-term averages during the whole period. However, due to its six satellite constellation system, FORMOSAT-3/COSMIC observes more atmospheric profiles than the sum of the other six missions.

Fig. 1 shows the number of RO atmospheric profiles per 5° bin in latitude or longitude for each mission, respectively. Note that, for better comparison, the number of FORMOSAT-3/COSMIC RO observations had been divided by 5 and the corresponding result was displayed in Fig. 1. As seen in Fig. 1, the zonal distribution of FORMOSAT-3/COSMIC data is approximately symmetric between the Northern Hemisphere (NH) and the Southern Hemisphere (SH) with four maxima around 50°S, 20°S, 20°N, and 50°N latitudes. Similar feature is also noted in the statistics of CHAMP, SAC-C, METOP/GRAS, and TerraSAR-X missions, while GRACE data seem to distribute more uniform between different latitudes and there are another two weak maxima appearing around 75°S and 75°N. Due to the 13° orbital inclination of C/NOFS satellites, C/NOFS observations are only distributed within 30°S–30°N, which facilitates tropical atmospheric exploration. The number of C/NOFS data reaches its maximum at the equator and then decreases with increasing latitude. It is seen in Fig. 1 that RO observations demonstrate uniform distribution in the longitudinal direction for all missions, with a weak wave-like structure found for FORMOSAT-3/COSMIC. The geographic locations of RO data depend on satellite orbit, which is primarily determined by mission requirements, e.g. scientific objectives. Therefore, combining data from more RO missions could result in a more even observation distribution.

In this study, we analyze the characteristics of thermal lapse-rate tropopause (LRT). It is defined as the lowest level at which the temperature lapse-rate is <2 K/km and the lapse-rate average between the level and the next 2 km does not exceed 2 K/km (WMO, 1957). However, in the polar regions, this definition would possibly cause problematic LRT results, because the temperature within the polar vortex usually keeps decreasing with height across the tropopause up to a height of about 20 km (Zängl and Hoinka, 2001). Hence, in order to remove the unrealistic LRTs determined by thermal definition, we apply a criterion at both poles similar to the one used by Schmidt et al. (2005). For regions poleward of 60° latitude, individual profiles are eliminated from the analysis if the temperature at the LRT level is below 195 K. In Fig. 2, the monthly percentage of unrealistic LRTs is presented over different zonal bands of polar regions. As seen in Fig. 2, over the Arctic,

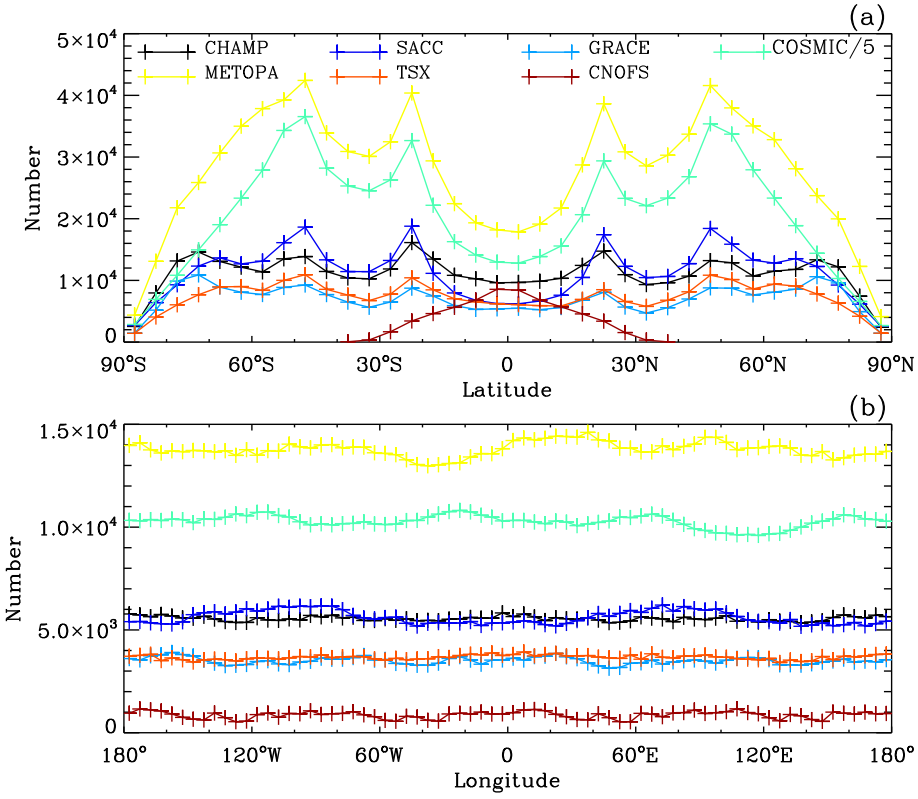

Fig. 1. Meridional (a) and zonal (b) distributions of RO profiles during the period between May 2001 and April 2013. The meridional and zonal resolutions are both 5°. The number of FORMOSAT-3/COSMIC RO observations shown in this figure represents only 1/5th of the realistic result.

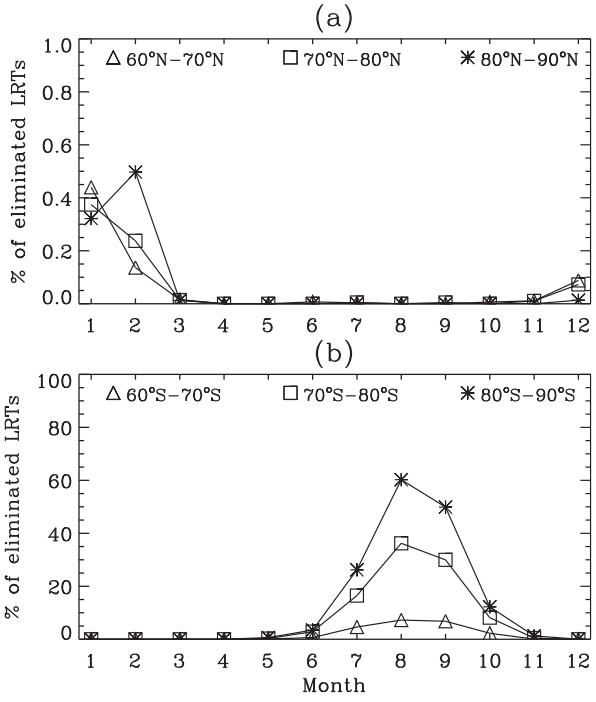

Fig. 2. Percentages of unrealistic LRTs in both polar regions.

the unrealistic LRTs are below 1% throughout the year, which implies that the Arctic polar vortex has little impact on the determination of LRT. Results are different for the south polar regions, showing considerable high percentages of unrealistic LRTs in June–September, which corresponds to the winter and early spring season of the SH. During this time, the Antarctic polar vortex usually reaches its highest strength and stability. This interhemispheric difference is because the Antarctic polar vortex is much more pronounced and persistent than the Arctic one. Based on the above two criteria, a total number of 5,874,973 LRTs have been successfully identified. Besides, only the first (lowest) LRT is considered in this study.

3. Intercomparisons between RO missions

The RO temperature profiles have shown good accuracy in extensive validation studies with numerical weather models (NWM), radiosonde observations, and other data sources (Wickert et al., 2004a; Gobiet et al., 2005; Kuo et al., 2005; Schmidt et al., 2008b; Fu et al., 2009; Sun et al., 2010; Zhang et al., 2011; Wang et al., 2013). It is found that throughout the upper troposphere and lower stratosphere, the temperature discrepancy is typically within 0.5 K in mean bias and 1–2 K in standard deviation. Theoretically, RO observations from different satellites or time periods can be used without inter-calibration for the self-calibration property of RO technique. However, in this section, we conduct an intercomparison of temperatures from different RO missions since such knowledge seems still lacking. Hajj et al. (2004) showed an average temperature difference of about 0.1 K between 5 and 15 km altitude for 212 pairs of nearby CHAMP and SAC-C occultations. We extend their study using a much larger RO data sample from seven RO missions.

Here, we perform data comparison between any two missions. Unfortunately, it is unable to present all the comparison results because RO observations from seven missions are used in this study and those lead to 21 combinations. Since FORMOSAT-3/COSMIC provides many more RO profiles than other missions, the following analyses are mainly about the statistical comparison results of RO data between FORMOSAT-3/COSMIC and the other six missions, respectively. In addition, the result of comparison between METOP/GRAS and TerraSAR-X is also shown. In all, comparison results of seven RO groups are considered, which are labeled as CHAMP–COSMIC, SACC–COSMIC, GRACE–COSMIC, METOPA–COSMIC, TSX–COSMIC, CNOFS–COSMIC, and METOPA–TSX for convenience. For all the groups, similar comparison method is adopted. Here, we take the CHAMP–COSMIC group as an example. CHAMP RO observations within 2 h and 200 km of FORMOSAT-3/COSMIC RO observations are compared to those from FORMOSAT-3/COSMIC. For each collocated pair, the temperature difference is calculated at all the vertical levels with data available, as shown in Equation (1):

$$\Delta T(h,\ i) = T_{CHAMP}(h,\ i) - T_{COSMIC}(h,\ i) \tag{1}$$

where $\Delta T(h,i)$ refers to the temperature difference between CHAMP and FORMOSAT-3/COSMIC; $T_{CHAMP}(h,i)$ and $T_{COSMIC}(h,i)$ refer to the temperatures of CHAMP and FORMOSAT-3/COSMIC, respectively; h is the altitude and i is the index of the collocated pair. The mean and standard deviation of ΔT are calculated and used to evaluate the discrepancy of CHAMP and FORMOSAT-3/COSMIC RO observations.

$$\overline{\Delta T(h)} = \frac{1}{n(h)} \sum_{i=1}^{n(h)} \Delta T(h,\ i) \tag{2}$$

$$SD_{\Delta T}(h) = \sqrt{\frac{1}{n(h)-1} \sum_{i=1}^{n(h)} \left(\Delta T(h,\ i) - \overline{\Delta T(h)}\right)^2} \tag{3}$$

where $\overline{\Delta T(h)}$ represents the mean temperature difference and $SD_{\Delta T}(h)$ represents the standard deviation of $\Delta T(h,i)$; $n(h)$ is the number of collocated pairs. Note that, a number of occultations could not penetrate down to the earth's surface due to abundant moisture, especially for tropical regions, so the number of collocated pairs usually varies with altitude.

Fig. 3 shows two examples of temperature profiles of collocated pairs, which locate in the middle and high latitudes, respectively. The observation times and graphic locations of these profiles are also demonstrated in Fig. 3. In each case, the FORMOSAT-3/COSMIC profile is

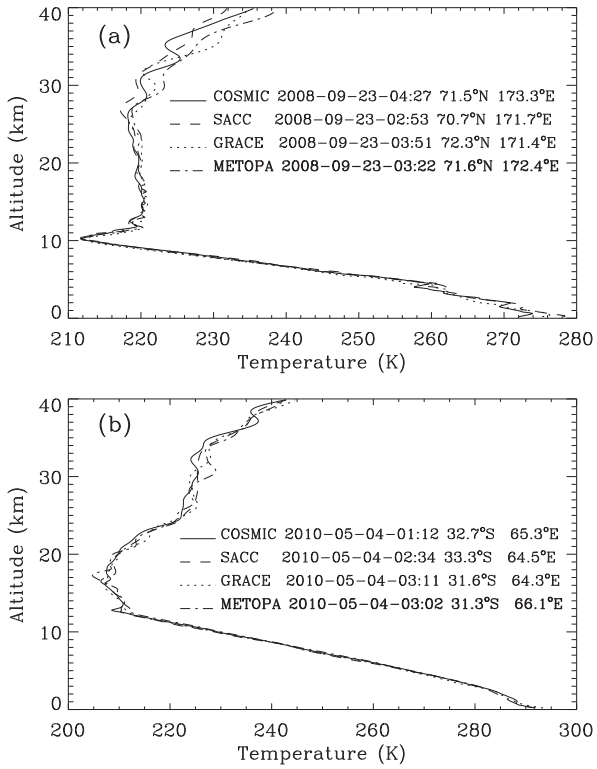

Fig. 3. Temperature profiles of FORMOSAT-3/COSMIC, SAC-C, GRACE, and METOP/GRAS.

synchronously matched with three profiles, respectively, from SAC-C, GRACE, and METOP/GRAS. As seen in Fig. 3, temperature profiles from the four missions show good agreement, especially between 5 and 25 km, whereas discrepancies begin to increase above 25 km. In Fig. 3a, over the Arctic, those four profiles locate very close to each other, and they demonstrate identical tropopause structure at around 10 km altitude. In contrast, Fig. 3b indicates the possibility of existing non-well defined tropopause or wave signature near tropopause, inferring the potential use of RO data for further investigations of tropopause characteristics and its nearby wave activities.

For each RO group, the global mean and standard deviation of temperature discrepancies at each vertical level between 0 and 40 km are presented in Fig. 4. The number of collocated pairs available for comparison at each vertical level is also given in Fig. 4c. Fig. 4c demonstrates similar features for all groups: below 10 km, the number of collocated pairs drops with decreasing altitude because of the poorer RO data quality in the lower troposphere; while above 10 km, it remains constant and is very close to the total number of collocated pairs (difference < 1%). As seen in Fig. 4, from 3 to 20 km altitude, the mean temperature differences for most RO groups are basically within 0.1 K with minimum values of ~0.03 K appearing at 14–15 km. Above 20 km, the absolute temperature bias increases to about 0.1–0.4 K with increasing altitude, and the RO groups METOPA–COSMIC and TSX–METOPA show more significant temperature biases than other groups. In the stratosphere, the atmospheric profiles of CHAMP, SAC-C, METOP/GRAS, and C/NOFS missions seem warmer than those of FORMOSAT-3/COSMIC, while the temperature profiles of GRACE is cooler. As noted in the lower stratosphere (20–35 km), METOP/GRAS shows warm biases of ~0.2–0.4 K compared to FORMOSAT-3/COSMIC or TerraSAR-X, almost two times the magnitude of biases obtained from other RO groups. Thus, this analysis indicates that above 20 km altitude METOP/GRAS temperature measurements show some discrepancy from other RO missions.

In Fig. 4b, it is found that the $SD_{\Delta T}$ curves of most RO groups completely overlap each other over the whole height range from the Earth's surface up to 40 km. Near the Earth's surface, $SD_{\Delta T}$ is as large as 3 K, but it quickly drops to about 2 K at 3 km height level. The lowest standard deviation is found at about 14 km with a value of ~1.2 K, and this coincides with the location of the lowest temperature bias. Then, from this level up to the top of the profile, $SD_{\Delta T}$ increases with increasing altitude to reach 3–4 K. However, there is an exception found in the features of the CNOFS–COSMIC group. Compared to the results of the other groups, CNOFS–COSMIC shows larger $\overline{\Delta T}$ values between 2 and 8 km altitude and smaller $SD_{\Delta T}$ values in the middle and upper troposphere and near the tropopause. Such disagreements should be attributed to the latitudinal variability in both $\overline{\Delta T}$ and $SD_{\Delta T}$, which are depicted in Figs. 5 and 6, respectively. As mentioned earlier, C/NOFS observations distribute only in the low latitudes, while results of the other RO groups shown in Fig. 4 represent global averages.

The above analyses indicate that throughout the troposphere and lower stratosphere, there exists no systematical bias in the temperature measurements from the seven RO missions examined in this study. Compared to the results of comparisons to NWM or radiosonde data, intercomparison of time-space matched RO profiles shows an obvious reduction in mean temperature differences, by about 80%, while, for the standard deviation of temperature differences, the RO intercomparison results show insignificant improvement. Best agreement of individual nearby RO profiles (lowest $\overline{\Delta T}$ and $SD_{\Delta T}$) is observed around the tropopause region, which is consistent with the comparison results of RO and other data sources.

The meridional distributions of means and standard deviations of SAC-C and FORMOSAT-3/COSMIC temperature differences are presented in Fig. 5, and similar results for METOP/GRAS and FORMOSAT-3/COSMIC are given in Fig. 6. In these two figures, the zonal mean results of $\overline{\Delta T}$ and $SD_{\Delta T}$ as well as the number of pairs are calculated in each 5° latitude bin. As seen in Fig. 5, between 5 and 7 km altitude, the temperature differences between SAC-C and FORMOSAT-3/COSMIC are positive for most latitudes, showing higher values (about 0.2–0.4 K) in the tropics than middle and high latitudes. Relatively higher discrepancy in the tropics is possibly due to the low accuracy of RO soundings caused by the abundant water vapor over this region, and this behavior is also observed in Fig. 6b as well as the results of RO groups not shown. It partly explains the apparent deviation of the $\overline{\Delta T}$ curve of CNOFS–COSMIC from those of other RO groups below 10 km altitude (Fig. 4a). It is surprised to notice in Fig. 6b that, the temperature differences between METOPA/GRAS and FORMOSAT-3/COSMIC demonstrate a distinct pattern above 7 km altitude, being positive in the SH and negative in the NH. From 8 km to 30 km altitude, the means of temperature differences vary from ~0 K to −0.5 K in the NH, and from 0–0.2 K to ~1.0 K in the SH. Reasons for this pattern are not clear currently, and this phenomenon is not found in the statistical results of RO groups not related to METOP/GRAS.

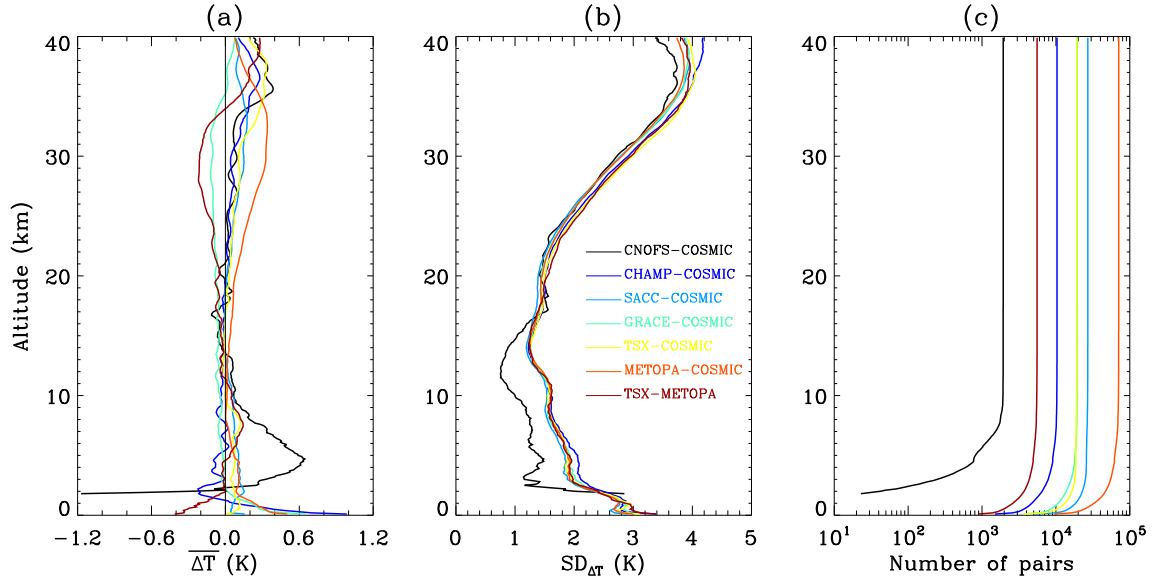

Fig. 4. Comparison of temperature profiles for seven RO groups. (a) Mean temperature differences. (b) Standard deviations of temperature differences. (c) Numbers of collocated RO pairs.

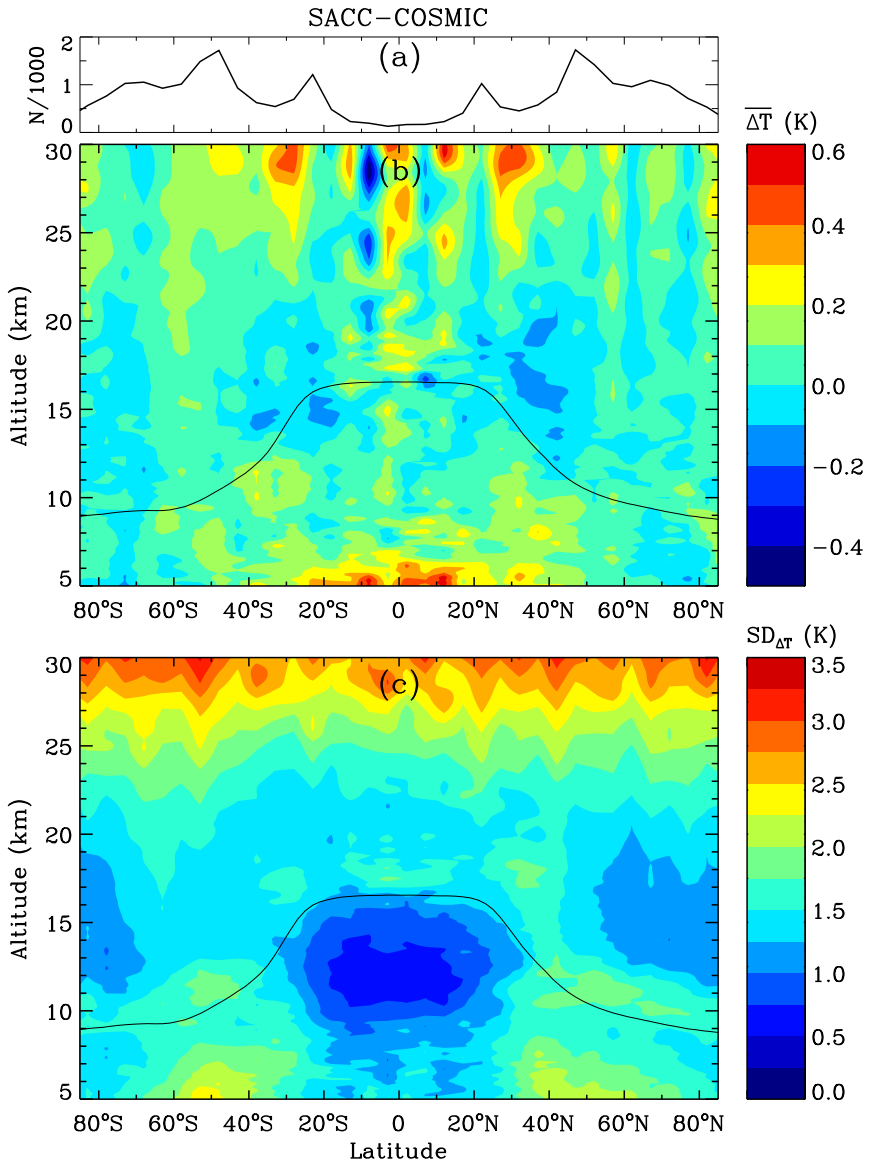

Fig. 5. Meridional variations (5° latitude interval) of (a) number of pairs, (b) mean, and (c) standard deviation of the temperature differences between SAC-C and FORMOSAT-3/COSMIC. The black lines in (b) and (c) show the meridional distribution of tropopause height.

From Figs. 5 and 6, it is observed similar latitudinal structures of $SD_{\Delta T}$ for SACC–COSMIC and METOPA–COSMIC. The lowest standard deviations of temperature differences are found to be <1 K over the tropics between 10 and 15 km altitude. This feature also explains the relatively lower $SD_{\Delta T}$ values of CNOFS–COSMIC shown in Fig. 4, since C/NOFS profiles are limited in the tropical regions. Below 20 km altitude, the standard deviations exhibit clear meridional difference with higher values around 2 K in the middle latitudes and lower values in the tropics and polar regions. Above 20 km altitude, the standard deviations are generally uniform for different latitudes. In addition, from the tropopause structure shown in Figs. 5 and 6, we can notice that in almost all the latitudes, there is an enhancement of standard deviations near or above the tropopause level, which may be associated with upper tropospheric variability. Such enhancement is also seen in the analyses of comparisons between RO and ECMWF data in both temperature and refractivity (Kuo et al., 2004; Xu et al., 2009).

In order to check the effect of collocation criteria on comparison results, Table 3 lists the mean temperature differences and standard deviations averaged between 5 and 25 km altitude for three different collocation criteria, including the one we have used and the other two with smaller distance limit and time window. In Table 3, Δd refers to the spatial buffer and Δt refers to the temporal buffer of collocation criteria; Num means the number of collocated pairs. On the whole, stricter collocation criteria result in no significant change in the statistical comparison results. $\overline{\Delta T}$ is found to remain constant for different spatial or temporal buffers, indicating that the temperature variability introduced by collocation criteria are irregular and always averaged to close to 0 K. $SD_{\Delta T}$ values show slight reduction when using stricter criteria, and the spatial buffer has more significant impact on the results than the temporal buffer.

4. Global tropopause characteristics from GPS RO

Twelve years of continuous RO soundings from seven missions have formed a comprehensive atmospheric data set for our study, and based on this data set, more detailed structure and variability of global tropopause are shown and discussed in this section. As known, the tropopause parameters exhibit apparent seasonal variation in most latitudes over the globe, although it is characterized by different patterns from tropical to extratropical regions. To detect such structure at a small spatial scale, we calculated the monthly means of zonal mean

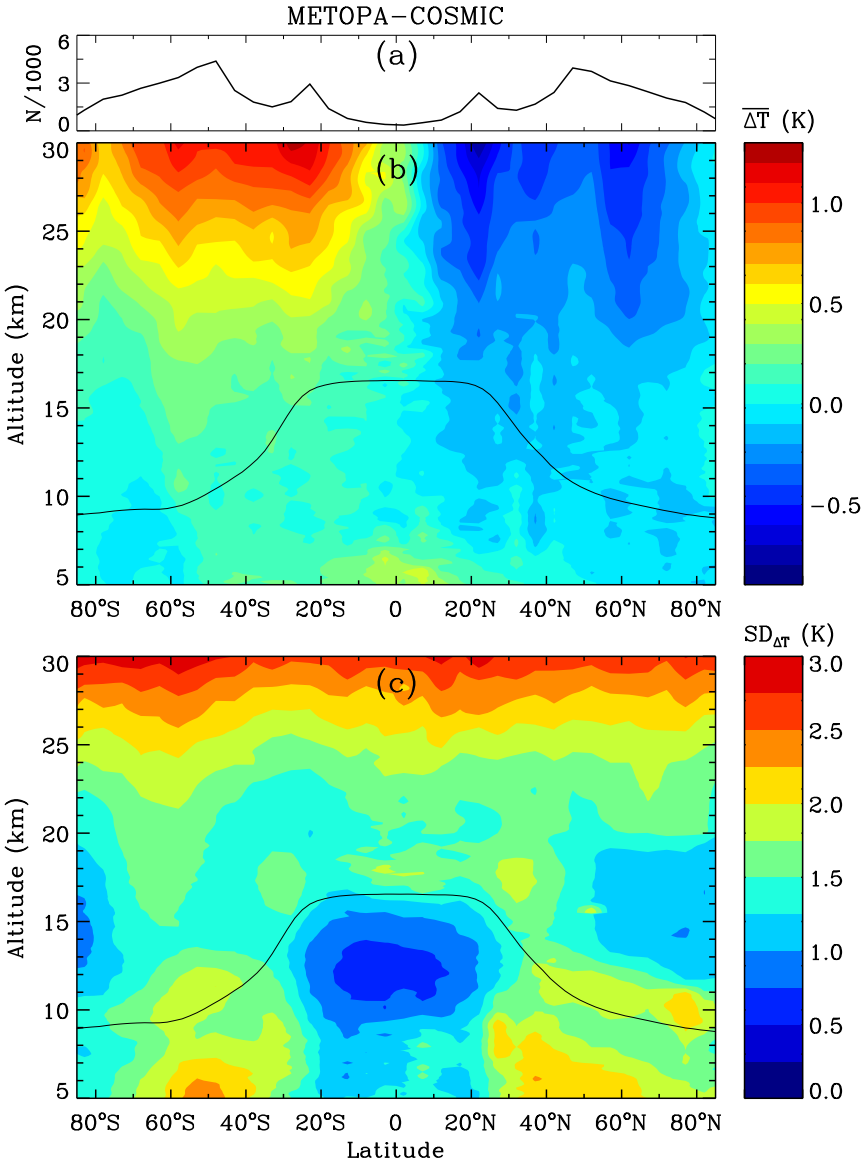

Fig. 6. Same as Fig. 5, but for METOPA–COSMIC.

tropopause altitude, pressure, and temperature as well as the corresponding standard deviations, in each 2° latitude band, as shown in Fig. 7a–f, respectively. Such high latitudinal resolution allows a better examination of tropopause seasonality in each small latitude band from the equator to the pole, as well as the transition of seasonal patterns in tropopause parameters. In general, standard deviations shown in Fig. 7d–e reflect the intramonthly variation of tropopause parameters. However, spatial difference might also play a role in the results, especially for regions showing remarkable zonal asymmetry in the tropopause structure. To acquire more specific information, the amplitudes (peak-to-peak values) of annual cycles from Fig. 7a–c are exhibited in Fig. 8. In Fig. 8, plus signs represent regions where tropopause altitude, pressure, and temperature show larger values in December–February (DJF) than in June–August (JJA), while triangles represent the opposite behavior. Spatial distributions of global tropopause parameters are presented in Fig. 9 for the DJF (NH winter) and JJA (NH summer) seasons,

Table 3
Mean temperature differences and standard deviations averaged between 5 and 25 km altitude and number of collocated pairs for the seven RO groups under three collocation criteria.

RO group	Δd < 200 km & Δt < 2 h			Δd < 100 km & Δt < 2 h			Δd < 100 km & Δt < 1 h		
	$\overline{\Delta T}$ (K)	*SD* (K)	Num	$\overline{\Delta T}$ (K)	*SD* (K)	Num	$\overline{\Delta T}$ (K)	*SD* (K)	Num
CHAMP–COSMIC	−0.01	1.57	10,247	−0.01	1.38	2667	−0.00	1.34	1440
SACC–COSMIC	0.03	1.48	26,864	0.03	1.26	6783	0.04	1.21	3719
GRACE–COSMIC	−0.06	1.53	19,300	−0.06	1.33	4818	−0.06	1.29	2548
TSX–COSMIC	0.03	1.56	19,074	0.04	1.37	4867	0.03	1.33	2645
METOPA–COSMIC	0.06	1.54	69,976	0.07	1.33	17,705	0.06	1.29	9459
CNOFS–COSMIC	0.08	1.27	1831	0.11	1.18	469	0.12	1.18	247
TSX–METOPA	−0.02	1.56	5499	−0.00	1.36	1359	−0.01	1.42	605

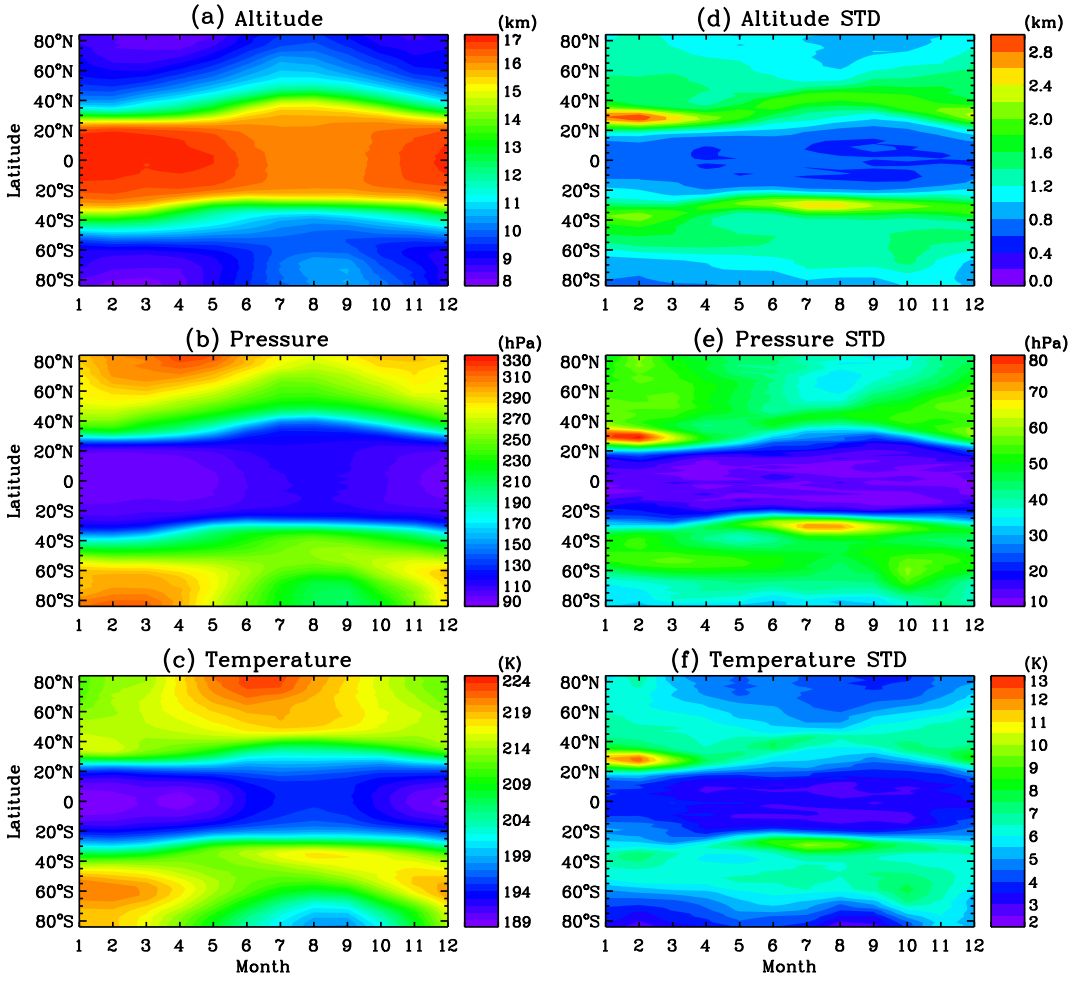

Fig. 7. Annual cycle of zonal mean tropopause altitude, pressure and temperature and standard deviations from seven RO missions listed in Table 1 for the period May 2001–April 2013.

respectively, in which the earth is divided into a uniform latitude-longitude grid with a resolution of 3° latitude by 5° longitude and the averages of tropopause parameters within each grid cell during the two seasons are calculated and shown. Each grid cell of Fig. 9 contains ~330 LRTs on the average. The high spatial resolution of Fig. 9 also allows a detailed view of global tropopause distribution, and is expected to reveal more reliable structures, such as the local extrema and high gradient of tropopause properties.

From Figs. 7–9, it is easy to obtain the following characteristics: (1) spatial structure. The tropopause ranges its altitude (pressure) from about 16–17 km (~100 hPa) in the tropics to about 8–9 km (~290 hPa) in the polar regions. The altitude (pressure) is almost constant between 20°S and 20°N, while outside the tropics it shows a poleward decrease (increase) with the strongest north-south gradients in the latitude belt of 25°–50° on both hemispheres, namely the subtropical jet stream area. The tropopause temperature has generally consistent meridional structure with altitude and pressure, but it also shows some different behaviors. For example, in the tropics it keeps increasing with latitude, and in the extratropics the maximum temperature gradients are found about 5° closer to the equator than those of altitude (pressure). The standard deviations of tropopause parameters are observed to be highest in the middle latitudes and lowest in the tropics during all the months; (2) seasonal variation. In both tropics and extratropics, distinct seasonal variations in tropopause parameters are found, whereas the pattern and amplitude both differ with respect to latitude, as can be seen in Figs. 7 and 8. Larger annual amplitudes appear in the vicinity of the subtropical jet stream regions as well as over the south polar regions. Generally, the zonal asymmetry of tropopause is more significant in winter than summer, such as the wave pattern found in the NH midlatitudes tropopause altitude (pressure) during DJF (Fig. 9a–b).

In summary, tropopause characteristics described above are in good agreement with previous statistical results derived from weather reanalysis data, radiosonde observations, or RO soundings. Therefore, in this study we will concentrate mainly on some new features of tropopause. Besides, a richer structure of tropopause for some specific regions is also revealed based on a large number of RO data.

4.1. Seasonal cycle

First, the seasonal cycles of tropopause parameters are discussed. As known, the tropical tropopause properties have a clear seasonal variation, in which temperature increases continually from January to August and then decreases, but it is noted from Fig. 7c that in fact this trend is not totally smooth for regions near the equator. Over a narrow equatorial belt, tropopause temperature shows an abrupt decrease in April and it reaches a value similar to that of January. Besides, we find this behavior is mainly restricted within an area of 5° on both sides of the equator. Studies have suggested that the seasonal cycle of tropical tropopause is determined by the stratospheric processes, for example the extratropical wave forcing (Reid and Gage, 1996; Highwood and Hoskins, 1998). And increased wave forcing occurring in NH winter tends to push the tropical tropopause altitude upward and lowers the temperature. Reid and Gage (1996) also pointed out that besides the winter peak, a maximum of the wave forcing might occur in April because at this time the combination of wave forcing from both

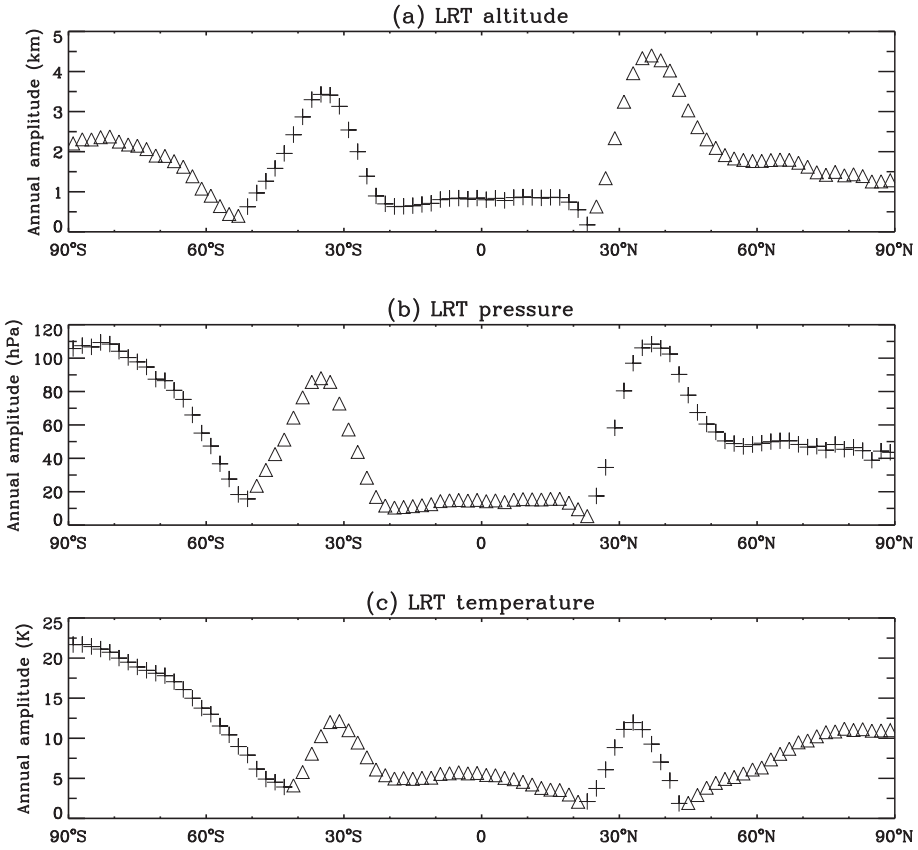

Fig. 8. Annual amplitude of zonal mean tropopause parameters (2° latitude interval). The plus signs represent regions where X_{LRT} (DJF) > X_{LRT} (JJA), while the triangles represent regions where X_{LRT} (DJF) < X_{LRT} (JJA). Here, X refers to the altitude, pressure, or temperature of tropopause.

hemispheres can reach another peak. Hence, the April minimum of tropopause temperature appearing only within 5° of the equator seems to support the theory of Reid and Gage (1996).

As seen in Fig. 7, the seasonal patterns of tropopause parameters differ between latitudes. In Fig. 8, the annual cycles of tropopause parameters are roughly classified into two types based on the difference of DJF and JJA values, which are represented using two kinds of symbols, respectively. Therefore, alternation of the two kinds of symbols could indicate the exact location where seasonal pattern transition occurs, namely, the phase reversal of annual cycle. Such information is useful for the identification of the major factors that determine annual variation, whereas they could not be acquired with low spatial resolution or irregular atmospheric observations. As seen in Fig. 7a–c and Fig. 8, the most prominent transition of the annual cycles in tropopause altitude, pressure, and temperature appears between 21°N and 23°N, and the seasonal variations of tropopause parameters on the north and south of this zone vary out of phase. It is also clearly seen in Fig. 8 that the reversal of annual cycle usually leads to local minimum amplitudes of tropopause parameters over the pattern transition zone. The extremely low annual amplitudes of tropopause parameters appearing around 23°N should result from the wintertime subtropical jet stream, which causes frequent occurrence of double tropopause over this region. As seen from Figs. 7a and 8a, for most tropical regions, the tropopause level is about 1 km higher in DJF than JJA, whereas double tropopause around 23°N tends to lower the altitude of tropopause during NH winter since the WMO definition only uses the lowest tropopause.

Another transition region for seasonal patterns of tropopause altitude (pressure) occurs between 53°S and 55°S (Fig. 7a–b and Fig. 8a–b), also accompanied with a local minimum of annual amplitude. In the extratropics, the transition zones for tropopause pressure and temperature behaviors do not coincide, and the pattern transition regions for tropopause temperature (Figs. 7c and 8c) are found to be symmetric about the equator, i.e. at 43°–45° on both hemispheres. However, we find characteristics for these two belts are totally different. Actually, low temperature amplitude found in 43°N–45°N represents a result of zonal average, because from Fig. 9c and f we can note that within this band, the seasonal oscillation of tropopause temperature shows remarkable asymmetric features in the zonal direction. For example, seasonal oscillations over the Pacific and Middle Asia are nearly out of phase with each other. Between 43°S and 45°S, in which the spatial structure of tropopause temperature is generally uniform during the entire year (Fig. 9c and f), the zonal mean results given in Figs. 7c and 8c can represent the general behavior of this zone. Previous studies have found that weak seasonal variability in tropopause pressure appears roughly at about 20°N and 50°S (Hoinka, 1998; Zängl and Hoinka, 2001). By using high spatial resolution RO data, this study gives more precise information on the features of the transition of annual cycle pattern in tropopause parameters.

As observed previously, the annual cycle of Arctic tropopause pressure exhibits two patterns: single wave in the Subarctic and double wave in the central Arctic (Highwood et al., 2000; Zängl and Hoinka, 2001). From Fig. 7b, we can see that the exact transition zone between these two patterns locates around 65°N. Single wave pattern prevails in the regions equatorward of 65°N while double wave pattern prevails in the regions northward of 65°N. In addition, the double wave pattern also shows slight differences between different altitudes. From 65°N latitude to the North Pole, appearance of the main peak of tropopause pressure changes from March to April, even May, and the second peak changes from November to October–November. It seems that as altitude increases, the time interval of the two peaks is getting smaller. Highwood et al. (2000) and Son et al. (2011) pointed out that the lower Arctic tropopause altitude (highest pressure) occurring in spring usually corresponds with the maximum intensity of high-latitude

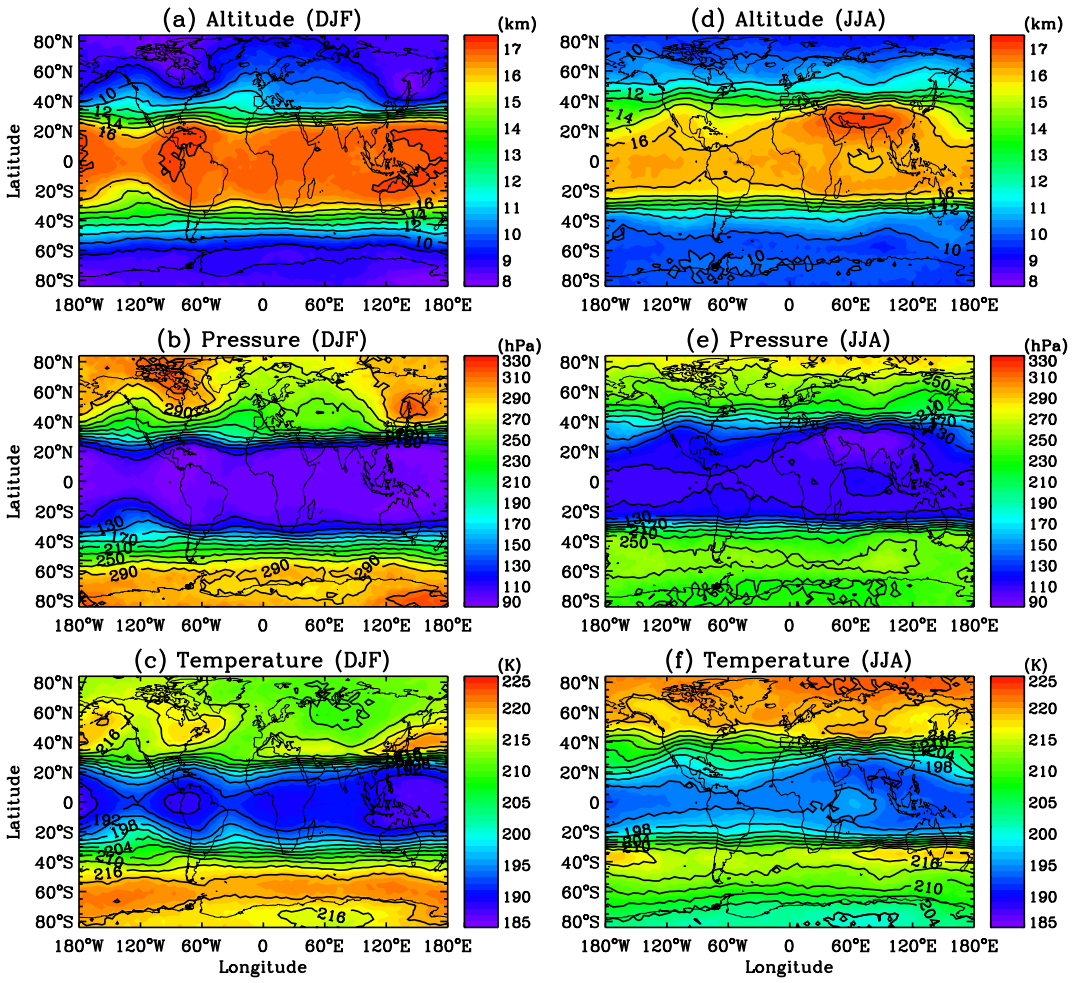

Fig. 9. Longitude-latitude section of seasonal mean tropopause altitude, pressure, and temperature during DJF and JJA from seven RO missions listed in Table 1 for the period May 2001–April 2013.

downwelling branch of Brewer-Dobson (BD) circulation during this time. Since it is always difficult to estimate the precise mass transport between stratosphere and troposphere, the detailed Arctic tropopause behaviors obtained from RO observations might be useful for reflecting the variation of BD circulation.

4.2. Spatial distribution

Based on the high resolution spatial structure of tropopause depicted in Fig. 9, some detailed characteristics over the tropics and both polar regions are analyzed in this section. First, the spatial distribution of tropical tropopause is discussed. It is seen in Fig. 9a–c that over the tropics, the lowest tropopause temperatures appear in the western tropical Pacific and northern part of South America during NH winter, and they generally coincide with the maxima of tropopause altitude (pressure); whereas in NH summer, the spatial distributions of different tropopause properties are not consistent. Those features are in good agreement with earlier studies by Highwood and Hoskins (1998) and Schmidt et al. (2004). But we also find in Figs. 9a and c that over the tropics the spatial extents of extreme tropopause temperatures and altitudes do not completely match each other during NH winter. For example, over the western tropical Pacific, low tropopause temperatures covers wider areas than high altitudes, for the former include the Indonesia archipelago and the latter show a horseshoe-shaped structure that extends along the north and south of Indonesia. A mismatch between tropopause parameters is also observed over the northern part of South America. Compared to the region of minimum temperature, the region of extreme altitude is extended to cover larger areas, including Central America and the eastern margin of tropical Pacific. Son et al. (2011) have described the active convective regions (annual mean) in the tropics (Fig. 2e of their paper), and pointed out that they approximately coincide with the extrema of tropopause parameters during NH winter. Santhi et al. (2014) presented a global morphology of atmospheric convection indices derived from FORMOSAT-3/COSMIC RO measurements for four seasons, respectively. Through comparison with their results, we note that those strong convections shown by Son et al. (2011) and Santhi et al. (2014) seem to demonstrate better match in spatial distribution with extrema of tropopause temperature than altitude (pressure). However, it is also found that the strong convections during DJF shown by Santhi et al. (2014) are mostly located between 0° and 15°S while the minima of tropopause temperature in Fig. 9c appear at the equator. Thus it indicates that besides convection, there are other factors influencing the spatial structure of tropical tropopause, especially for tropopause altitude.

We next concentrate on the spatial distribution of the tropopause parameters over both poles, which have not been studied in detail through RO observations. As already mentioned in Section 2, the problematic polar tropopauses due to the thermal definition were eliminated from the statistics to avoid unrealistic structure. It is seen in Fig. 2b that over the central Antarctic region, the maximum percentage of problematic LRTs reaches above 35% (65% for areas > 80°S) in August, whereas the percentage remains below 20% during October–June. Over the Arctic, the problematic LRTs are always negligible during all the months. At first, the tropopause in the NH polar region is explored.

During DJF season, the maximum tropopause pressure (temperature) reaching about 310 hPa (216 K) appears at about 60°N, 90°W, over the Canadian Arctic Archipelago, as seen in Fig. 9b–c. Lower pressure (temperature) with values between 260 and 270 hPa (210 − 212 K) is found over the northern Atlantic, Nordic Europe, and western Siberia. During JJA season, the Arctic tropopause shows obviously less zonal variation, while its meridional gradient becomes more remarkable than in DJF. Because in this period, the tropopause pressure increases approximately from 250 hPa at 60°N to 290 hPa at 90°N, and the temperature ranges between 219 and 222 K.

Compared to the Arctic, tropopause parameters over the Antarctic exhibit less spatial structures, and the local extreme values are also less significant, as observed in Fig. 9. Throughout the year, the Antarctic tropopause structure usually demonstrates zonal symmetry. But the winter-summer difference is much stronger in the Antarctic than in the Arctic, which is also seen in Figs. 7 and 8. During DJF season, tropopause pressure over the Antarctic varies from 280 to 310 hPa, and temperature varies from 216 to 221 K. Weak extrema are found in small areas near the South Pole, but the extreme pressure and temperature do not coincide spatially, for the pressure shows a maximum (310 hPa) between 120°E and 160°W around 80°S latitude, while the temperature shows a minimum (below 216 K) between 30°E and 100°E around 80°S latitude. During JJA season, the Antarctic tropopause becomes more zonally symmetric, with pressure ranging between 230 and 260 hPa. Compared to DJF, temperature shows stronger north-south gradient in JJA, with values decreasing from ~210 K at 60°S latitude to ~203 K near the South Pole.

The structure of RO-derived polar tropopause described above are similar to those of the dynamical tropopause presented by Hoinka (1998, 1999), especially in terms of local extremes. Although the meaning of such comparison is somewhat limited by the fact that the periods of those data used in different studies do not overlap, we may still conclude that, on the whole, the two tropopause definitions lead to similar structures for all the seasons in the Arctic. Therefore, thermal definition is suitable to investigate the Arctic tropopause using RO data. Above the Antarctic, the thermal tropopause is also unproblematic in austral summer. For austral winter, due to the uniform and zonally symmetric features of the Antarctic tropopause in this period, the selected LRTs can depict seasonal mean structure approximately similar to that of the dynamical definition, though the percentage of eliminated LRTs is relatively high. Further study of the Antarctic tropopause over the polar vortex is needed.

4.3. Interannual variation

Based on multiple occultation missions, long-term time series of tropopause parameters are obtained from May 2001 to April 2013. Figs. 10–12 show the monthly evolutions of zonal mean tropopause temperature during the whole period over the equatorial band between 10°S and 10°N, middle latitudes between 30°N and 40°N, and central Arctic regions between 70°N and 80°N, respectively. In order to investigate the relationship between tropopause and the atmospheric property below or above it, the time series of monthly mean zonal mean temperatures in the upper troposphere and lower stratosphere are also presented for the three regions in Figs. 10–12, respectively. For a more explicit analysis, monthly anomalies of zonal mean temperatures at tropopause level and in the upper troposphere and lower stratosphere are calculated by subtracting the annual cycle from each monthly mean, similar to the method used by Seidel et al. (2001) and Schmidt et al. (2008a).

As seen from Fig. 10b, in the equatorial regions, the tropopause temperature shows obvious interannual characteristics, with more significant magnitude in NH winter than NH summer. In NH winter, the absolute tropopause temperature anomalies mostly reach up to 0.5–1.5 K, whereas in NH summer they decrease to below 0.5 K. During the entire observation period, the most prominent tropopause temperature anomaly reaching about 2 K appears in 2010–2011 winter, and it was also observed in cold point tropopause over the tropics by Kumar et al. (2014). There also exists a temperature anomaly of − 1 K in the summer of 2010. As noted from Fig. 10a–b, the interannual variation of equatorial tropopause temperature shows close agreement with that of temperature in the lower stratosphere (at 18 or 20 km), which is consistent with earlier studies derived from radiosonde observations (Seidel et al., 2001). In Fig. 10a–b, signature of QBO is observed in the time series of temperature both at tropopause and in the lower stratosphere, especially at 20 km altitude. It is usually suggested that the temperature anomaly pattern at tropopause is formed by the stratospheric

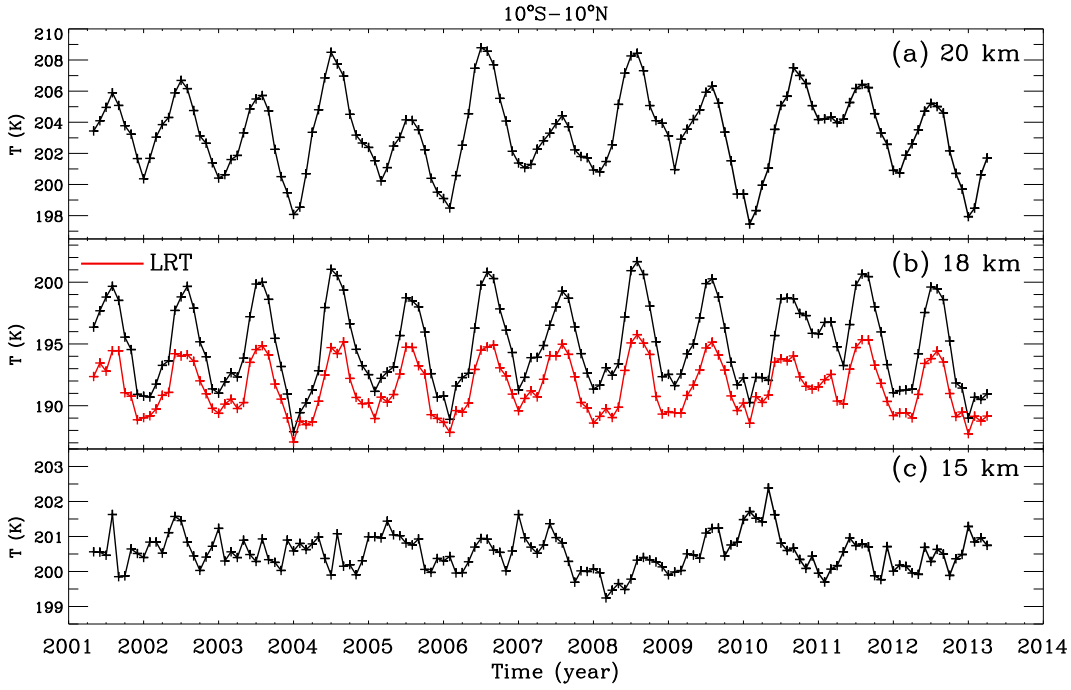

Fig. 10. Time series of monthly averaged temperature at (a) 20 km, (b) 18 km, (c) 15 km altitude, and tropopause (red line in (b)) over the equator regions (10°S–10°N) derived from seven RO missions listed in Table 1 for the period May 2001–April 2013.

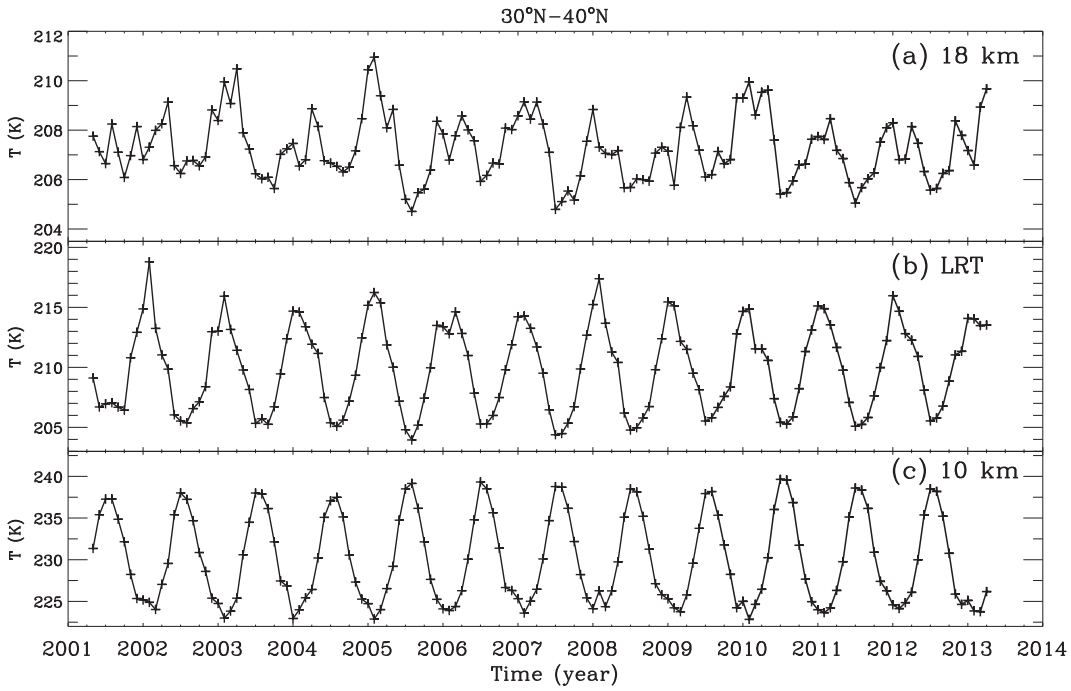

Fig. 11. Time series of monthly averaged temperature at (a) 18 km, (b) tropopause, and (c) 10 km altitude over the middle latitude region (30°N–40°N) derived from seven RO missions listed in Table 1 for the period May 2001–April 2013.

QBO (Schmidt et al., 2005). But as found in Fig. 10a–b, the influence of QBO is less strong in NH summer, for at this time the tropopause temperature anomalies show less correlation with temperature anomalies at 18 or 20 km than in NH winter. Temperature in the upper troposphere (at 15 km) exhibits generally weak temporal variations with a standard deviation of only 0.5 K for the whole period, and it seems to show little correlation with the tropopause temperature. But during spring and summer of 2010, a distinct peak that is about 1.3 K higher than the annual mean value is noted for the tropospheric temperature. Whether this abnormality has some relationship to the remarkable tropopause temperature anomalies during 2010–2011 needs a further investigation.

It is seen in Fig. 11b that tropopause temperature between 30°N and 40°N shows less significant interannual variation than that in the tropics, although the seasonality is much more remarkable in the middle latitudes. Over this zone, the tropospheric temperature (at 10 km) in

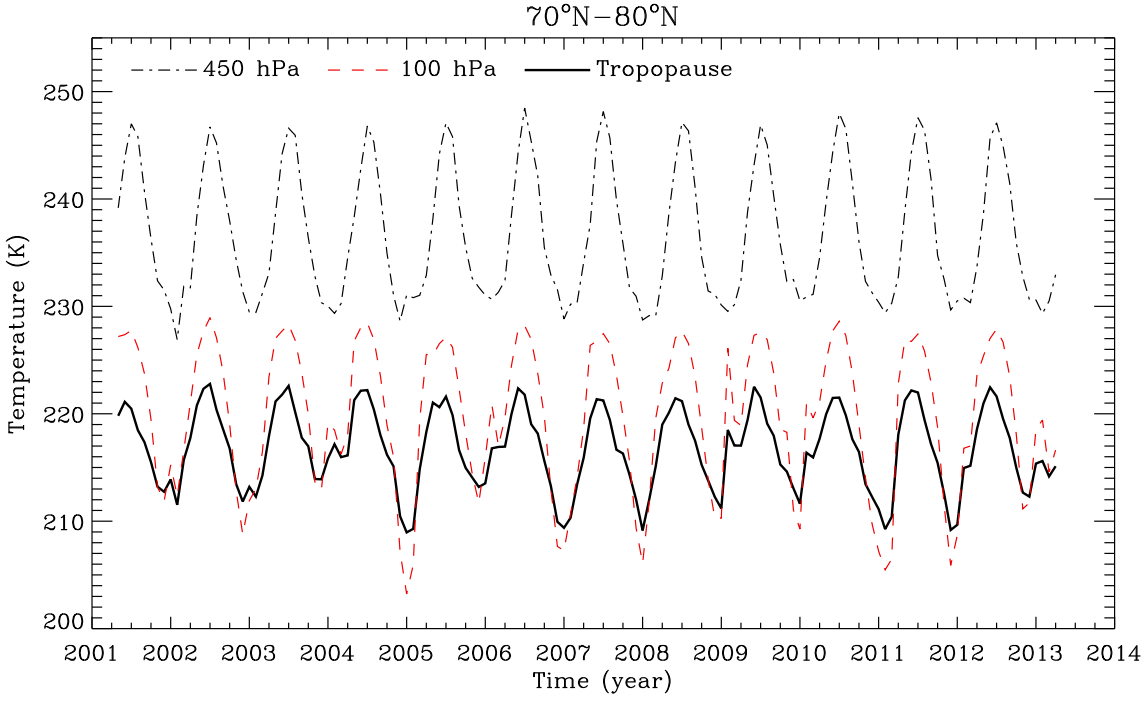

Fig. 12. Time series of monthly averaged tropopause temperature and temperature at 450 and 100 hPa over the Arctic region (70°N–80°N) derived from seven RO missions listed in Table 1 for the period May 2001–April 2013.

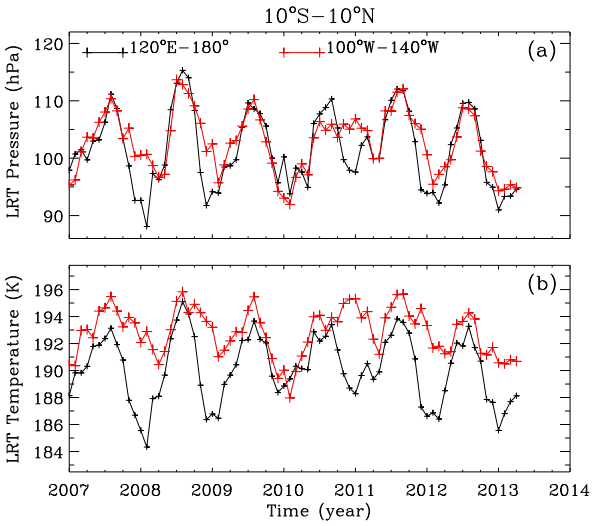

Fig. 13. Time series of monthly averaged tropopause pressure and temperature over two regions within the equator (10°S–10°N) for the period January 2007–April 2013.

Fig. 11c has a constant annual cycle with little year-to-year variation; while the stratospheric temperature (at 18 km) in Fig. 11a demonstrates relatively complex temporal characteristics, showing oscillations at both the annual and semiannual periods. From Fig. 11, it is found obviously no correlation between the tropopause temperature with temperatures either below or above the tropopause for this middle latitude band.

In the central Arctic the interannual variation of tropopause temperature is more significant compared to the equatorial and middle latitude regions, as shown in Fig. 12. Similar to the results near the equator, the Arctic tropopause has larger anomalies in NH winter than NH summer, being mostly ~0.5–4 K in winter and <0.5 K in summer. Note that the annual cycle of tropospheric temperature (at the 450 hPa level) remains generally constant during the entire observation period, while for stratospheric temperature (at the 100 hPa level), dramatic interannual variation is usually observed during DJF season. Zängl and Hoinka (2001) pointed out that the annual cycle of polar tropopause pressure is closely related with the temperature difference between upper troposphere and lower stratosphere. However, we can notice in Fig. 12 that the interannual variation of Arctic tropopause temperature usually correlates with that of temperature in the lower stratosphere, and no relation with tropospheric temperature is found. Prominent anomalies of temperature at tropopause and 100 hPa level include warming events in 2003–2004 winter, 2005–2006 winter and 2008–2009 winter, and a few cooling events in 2004–2005 winter, 2007–2008 winter, 2011–2012 winter, etc. Those warming events are normally considered to be related with the Arctic winter warming in the lower and middle stratosphere. Dhaka et al. (2015) studied detailedly the Sudden Stratospheric Warming events occurred in January 2009 using FORMOSAT-3/COSMIC RO data and found a strong dynamical coupling between the polar and tropical regions. However, the simultaneous cooling of stratospheric temperature over the tropical regions shown by Dhaka et al. (2015) is not observed in Fig. 11a and b. That's because the cooling is more remarkable in the middle stratosphere while its magnitude decays as altitude decreases and reaches only about 2 K in tropopause region, as shown by Dhaka et al. (2015). Besides, the results of Fig. 11 represented monthly averages, which tend to smooth such sudden fluctuation.

In previous studies, the interannual characteristics of tropopause are usually investigated based on zonal mean properties due to limited and sparse atmospheric observations. The high spatial resolution and even coverage of RO data set from multiple missions enables a further analysis for different longitudes. Since the RO observations were relatively sparse before the launch of FORMOSAT-3/COSMIC satellites, this analysis is performed using observations after 2006. In Fig. 13, the temporal variations of tropopause pressure and temperature from January 2007 to April 2013 are shown for two localized tropical regions within 10°S–10°N, respectively. The two chosen regions are: the western tropical Pacific warm pool region (120°E–180°) and the eastern tropical Pacific (100°W–140°W), where tropopause over the latter is warmer than other equatorial regions during DJF (see Fig. 9c). The warm pool is crucial for tropical tropopause, since it is suggested as the main region where tropospheric air parcels enter the stratosphere for its low tropopause temperature caused by deep convection (Highwood and Hoskins, 1998). As clearly seen in Fig. 13, tropopause parameters over the two regions reveal substantially different characteristics in interannual variation. For example, in 2010–2011 winter, tropopause temperature of western tropical Pacific shows an anomaly of ~1 K while this value reaches as high as 6 K for eastern tropical Pacific. Thus, it indicates that the remarkable tropopause anomaly during 2010–2011 winter shown in Fig. 10b is primarily due to behaviors outside the warm pool.

Table 4 presents correlations between monthly temperature anomalies at tropopause and those in the upper troposphere and lower stratosphere during the period between January 2007 and April 2013. Corresponding results for the whole equatorial band 10°S–10°N and two spatially localized regions near the equator mentioned above are shown in Table 4, respectively. Although interannual characteristics of equatorial tropopause demonstrate remarkable zonal differences, it is seen from Table 4 that close correlation between tropopause temperature and stratospheric temperature is found in both regional and zonal mean structures, with correlation coefficients of 0.86, 0.77, and 0.86 respectively. The correlation analyses for the middle latitudes and Arctic regions are also shown in Table 4, which will be discussed below.

The temporal characteristics of tropopause parameters in two regions located within the middle latitude band 30°N–40°N are presented in Fig. 14, respectively. The two chosen regions are: the east of China and Japan (90°E–150°E), where intensive subtropical jet stream is usually found in winter, and the western Pacific region (120°W–180°), where jet stream has less strength. It is easily found in Fig. 14 that the interannual variations of tropopause properties are more noticeable in the vicinity of strong jet stream, in which wintertime temperatures (pressure) show a decrease from 2008 to 2010 and then an increase from 2010 to 2012. From Table 4, we find little correlation between tropopause temperature and temperature below or above for these two middle latitude regions, similar to the behaviors of zonal mean properties mentioned previously. In addition, it is noted from Fig. 14b that the annual cycle of tropopause temperature for the region 120°W–180° has a double-wave pattern, being warmer in NH winter and summer and cooler in spring and autumn. This is different from the feature of the zonal mean tropopause temperature shown in Fig. 7c.

Table 4
Correlation coefficients among monthly anomaly time series of tropopause temperature and tropospheric and stratospheric temperatures, derived from RO data for the period January 2007–April 2013. T_{LRT}' refers to monthly temperature anomalies at the LRT; T_{stra}' and T_{tro}' refer to monthly temperature anomalies in the lower stratosphere and upper troposphere, respectively.

	10°S–10°N	10°S–10°N 120°E–180°	10°S–10°N 100°W–140°W	30°N–40°N	30°N–40°N 90°E–150°E	30°N–40°N 120°W–180°	70°N–80°N	70°N–80°N 80°W–140°W	70°N–80°N 0°–60°E
T_{LRT}' & T_{stra}'	0.86	0.77	0.86	0.18	0.06	0.39	0.94	0.82	0.92
T_{LRT}' & T_{tro}'	0.00	0.11	0.14	−0.03	0.34	−0.10	0.21	0.11	−0.02

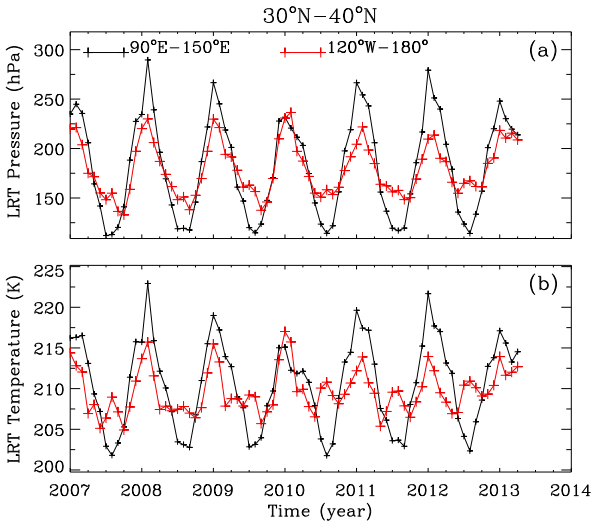

Fig. 14. Time series of monthly averaged tropopause pressure and temperature over two regions in the middle latitudes (30°N–40°N) for the period January 2007–April 2013.

The temporal characteristics of tropopause parameters over two regions located within the central Arctic (70°N–80°N) are presented in Fig. 15, respectively. The two chosen regions are: the northeastern part of Canada (80°W–140°W), where a maximum of tropopause temperature is observed during NH winter, and the Nordic Europe (0°–60°E). From Fig. 15a, seasonal variations in tropopause pressure show a similar bimodal pattern over both local regions between 70°N and 80°N, which is similar to the results given by Zängl and Hoinka (2001). Interannual tropopause temperature anomalies are greater over 0°–60°E, and they are also uncorrelated with the anomalies over 80°W–140°W, especially for NH winter season. As found in Table 4, the relationship between tropopause temperature and stratospheric temperature in the central Arctic is similar to that in the tropics, but with even higher correlations. We calculated the average number of monthly LRTs during the entire period between January 2007 and April 2013, and this value varies from 454 to 893 for the six local regions shown in Figs. 13–15.

4.4. Diurnal variation

Fig. 16a–b presents the diurnal variation of equatorial tropopause (within 10°S–10°N) characteristics in January and August, respectively. It is obtained through converting the UTC (Coordinated Universal Time) of RO observations into local times and then calculating the means of tropopause parameters for each individual hour. The number of LRTs used to calculate the diurnal variation is given in Fig. 16c, and it indicates similar features for January and August. The highest number of LRTs (~2700) occurs around 10 a.m. local time and the lowest number (~1000) occurs at midnight. It is observed from Fig. 16a that in January, the tropopause parameters show a clear diurnal variation. Tropopause temperature peaks at about 07:00–11:00 a.m. local time and then it decreases to its minimum at midnight, showing an amplitude of 1.2 K. Tropopause altitude demonstrates consistent temporal variation features with temperature, with a diurnal amplitude of 0.16 km. However, in August, the diurnal variation becomes more irregular although less strong, with amplitudes of only 0.1 km and 0.5 K for tropopause altitude and temperature, respectively. In August, the tropopause temperature shows a maximum in the morning, and during the rest time of the day it shows a wave-like variation. Compared to the characteristics in January, the extreme tropopause altitudes appear a few hours earlier in August, being lowest at 05:00–07:00 and highest at 20:00 local time.

5. Summary and discussion

This study presents a comprehensive analysis on the temporal and spatial structure of global lapse-rate tropopause using a combined data set from seven RO measurement missions for 12 years. Based on such high spatiotemporal resolution observations, new climatological characteristics and more detailed structures are obtained. Main findings of our study are summarized below.

Statistical intercomparison of temperature measurements between different RO missions have shown similar results for most RO groups except for COSMIC–CNOFS, because C/NOFS measurements only distribute in the tropics. The mean temperature differences between 5 and 25 km altitude are within ±0.1 K, and standard deviations are 1.48–1.57 K; best agreement is found at 14–15 km altitude, near the tropopause region, with a mean temperature difference of 0.03 K and standard deviation of 1.23 K. Below 20 km altitude, standard deviations of temperature difference show distinct meridional variation, with highest values in the middle latitudes and lowest values in the tropics. An increase of standard deviation near or above the tropopause level is observed for most latitudes.

The annual cycle of tropical tropopause temperature shows a second minimum during April in a narrow belt within about 5° of the equator, which may be related to the maximum of wave forcing combination from two hemispheres in this month. The precise transition zones for seasonal patterns of tropopause parameters are found to be located in 21°N–23°N and 53°S–55°S for pressure, and 21°N–23°N, 43°–45° latitudes on both hemispheres for temperature. The seasonal characteristics of tropopause temperature over the NH middle latitudes reveal remarkable asymmetry in the zonal direction. In the central Arctic where bimodal annual cycle of tropopause pressure prevails, the time interval of the two peaks is found to become smaller as altitude increases.

In the tropics, the spatial extents of extreme tropopause temperature and altitude do not totally coincide and temperature extrema demonstrate better match with the strong convection than altitude extrema. Detailed structures of thermal tropopause over the Arctic and over the Antarctic during its summertime are found to be consistent with the characteristics of the dynamical tropopause, which indicates that the thermal definition is suitable for describing the Arctic tropopause and summertime Antarctic tropopause by RO measurements.

Interannual characteristics of tropopause temperature over the equator, the NH middle latitudes, and central Arctic are shown, respectively. Clear interannual variation is observed in all three latitude zones,

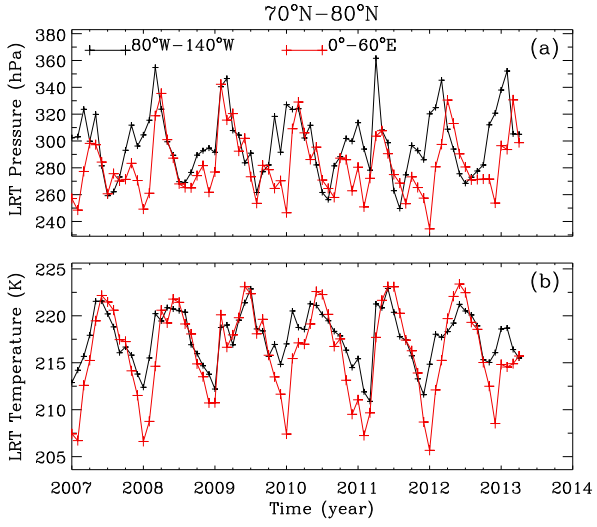

Fig. 15. Time series of monthly averaged tropopause pressure and temperature over two regions in the central Arctic (70°N–80°N) for the period January 2007–April 2013.

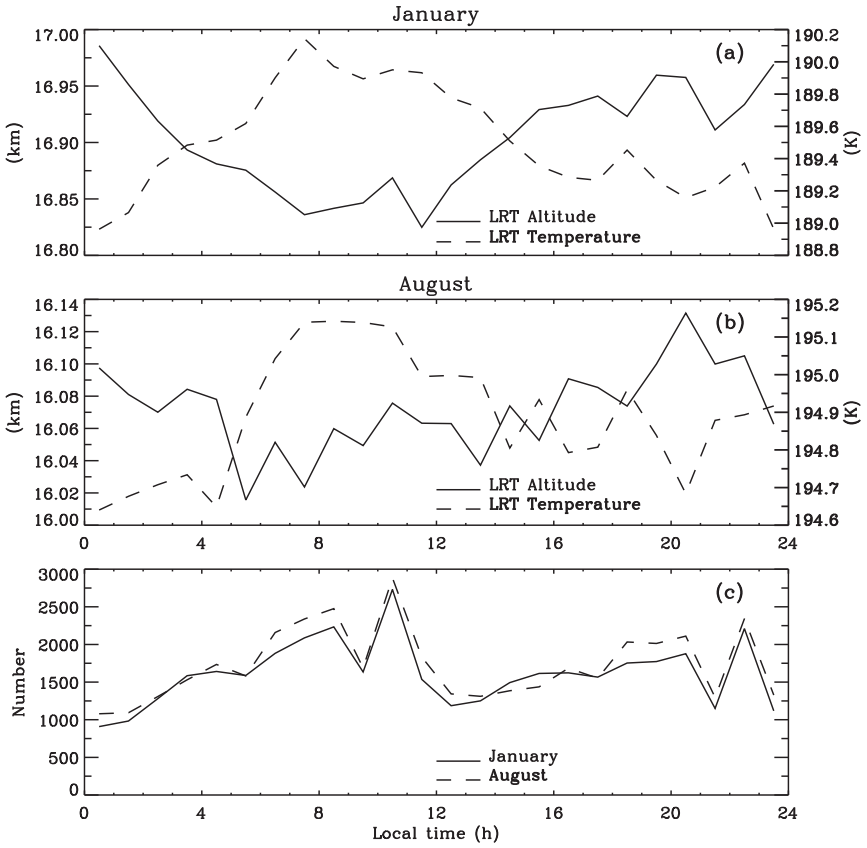

Fig. 16. Diurnal variations of tropopause altitude, temperature, and number of LRTs in January and August for the equatorial region 10°S–10°N, respectively.

with much greater amplitude in the Arctic and relatively lower amplitude in the middle latitude zone. Besides, tropopause temperature anomalies are more predominant in NH winter than in summer for both tropics and Arctic. For all three latitude bands, the interannual behaviors of tropopause parameters exhibit apparent zonal asymmetries and deserve further investigation. Close agreement between monthly temperature anomalies at tropopause and in the lower stratosphere are noted in both the tropics and high latitudes, and such a strong correlation exists for both local and zonal mean temperatures. In the middle latitudes, little correlation between tropopause temperature and atmospheric temperature below or above is found.

Diurnal characteristics of the equatorial tropopause shows that: in January, the tropopause is warmer in the morning and cooler at midnight, with a consistent variation observed in tropopause altitude; while for August the diurnal variations become lower but more complicated.

It should be noted that, although this study has revealed some new and detailed structures of tropopause from multiple RO observations, the corresponding physical mechanisms have not been deeply investigated. As we have also found, the spatiotemporal resolution used in our figures are still not high enough to detect sudden events, for example, the tropical tropopause cooling during January–February 2009. Our future work will further concentrate on specific characteristics in smaller spatial scale and shorter time span and discuss related dynamical or radiative processes near the tropopause. In addition, expect for climate change and tropospheric–stratospheric exchange, the tropopause may also play a role in other atmospheric processes. For instance, Bonafoni and Biondi (2016) found that the cold point tropopause identified by RO profiles can be used as an indication of cloud top height of precipitation events. Thus, investigation of the relationship with other dynamics in the troposphere and stratosphere will also help to extend our knowledge about tropopause.

Acknowledgements

The authors are grateful to the CDAAC for providing radio occultation data. This work was supported by the National key Research Program of China “Collaborative Precision Positioning Project” (No. 2016YFB0501900) and the National Natural Science Foundation of China (41104103, 41574032, 41231064, 41174031).

References

Anthes, R.A., Bernhardt, P., Chen, Y., Cucurull, L., Dymond, K., Ector, D., Healy, S., Ho, S., Hunt, D., Kuo, Y., Liu, H., Manning, K., McCormick, C., Meehan, T.K., Randel, W.J., Rocken, C., Schreiner, W.S., Sokolovskiy, S.V., Syndergaard, S., Thompson, D.C., Trenberth, K.E., Yen, N.L., Zeng, Z., 2008. The COSMIC/FORMOSAT-3 mission: early results. Bull. Am. Meteorol. Soc. 89 (3), 313–333.

Bonafoni, S., Biondi, R., 2016. The usefulness of the Global Navigation Satellite Systems (GNSS) in the analysis of precipitation events. Atmos. Res. 167, 15–23.

Dhaka, S.K., Kumar, V., Choudhary, R.K., Ho, S.P., Takahashi, M., Yoden, S., 2015. Indications of a strong dynamical coupling between the polar and tropical regions during the sudden stratospheric warming event January 2009, based on COSMIC/FORMASAT-3 satellite temperature data. Atmos. Res. 166, 60–69.

von Engeln, A., Andres, Y., Marquardt, C., Sancho, F., 2008. GRAS status and future European radio occultation missions. GRAS SAF Workshop on Applications of GPSRO Measurements, Reading, UK, 16–18 June 2008.

von Engeln, A., Andres, Y., Marquardt, C., Sancho, F., 2011. GRAS radio occultation onboard of Metop. Adv. Space Res. 47 (2), 336–347.

Foelsche, U., Borsche, M., Steiner, A.K., Gobiet, A., Pirscher, B., Kirchengast, G., Wickert, J., Schmidt, T., 2008. Observing upper troposphere–lower stratosphere climate with radio occultation data from the CHAMP satellite. Clim. Dyn. 31 (1), 49–65.

Fong, C.J., Shiau, W.T., Lin, C.T., Kuo, T.C., Chu, C.H., Yang, S.K., Yen, N.L., Chen, S.S., Kuo, Y.H., Liou, Y.A., Chi, S., 2008a. Constellation deployment for the FORMOSAT-3/COSMIC mission. IEEE Trans. Geosci. Remote Sens. 46 (11), 3367–3379.

Fong, C.J., Yang, S.K., Chu, C.H., Huang, C.Y., Yeh, J.J., Lin, C.T., Kuo, T.C., Liu, T.Y., Yen, N.L., Chen, S.S., Kuo, Y.H., Liou, Y.A., Chi, S., 2008b. FORMOSAT-3/COSMIC constellation spacecraft system performance: after one year in orbit. IEEE Trans. Geosci. Remote Sens. 46 (11), 3380–3394.

Fong, C.J., Yen, N., Chu, V., Yang, E., Shiau, A., Huang, C.Y., Chi, S., Chen, S.S., Liou, Y.A., Kuo, Y.H., 2009. FORMOSAT-3/COSMIC spacecraft constellation system, mission results and prospect for follow-on mission. Terr. Atmos. Ocean. Sci. 20 (1), 1–19 (Feb. 2009).

Fu, E.J., Zhang, K.F., Marion, K.Y., Xu, X.H., Marshall, J., Rea, A., Weymouth, G., Kuleshov, Y., 2009. Assessing COSMIC GPS radio occultation derived atmospheric parameters using Australian radiosonde network data. Proceed. Earth Plan. Sc. 1 (1), 1054–1059.
Gettelman, A., Forster, P.M.D., 2002. A climatology of the tropical tropopause layer. J. Meteorol. Soc. Jpn. 80 (4B), 911–924.
Gobiet, A., Foelsche, U., Steiner, A.K., Borsche, M., Kirchengast, G., Wickert, J., 2005. Climatological validation of stratospheric temperatures in ECMWF operational analyses with CHAMP radio occultation data. Geophys. Res. Lett. 32 (12).
Hajj, G.A., de la Torre Juárez, M., Iijima, B.A., Mannucci, A.J., Yunck, T.P., 2002. GPS radio occupations coming of age: spacecraft launches add two new instruments for climate monitoring. EOS Trans. Am. Geophys. Union 83 (4), 37.
Hajj, G.A., Ao, C.O., Iijima, B.A., Kuang, D., Kursinski, E.R., Mannucci, A.J., Meehan, T.K., Romans, L.J., Juarez, M.D., Yunck, T.P., 2004. CHAMP and SAC-C atmospheric occultation results and intercomparisons. J. Geophys. Res. 109 (D6).
Highwood, E.J., Hoskins, B.J., 1998. The tropical tropopause. Q. J. R. Meteorol. Soc. 124 (549), 1579–1604.
Highwood, E.J., Hoskins, B.J., Berrisford, P., 2000. Properties of the Arctic tropopause. Q. J. R. Meteorol. Soc. 126 (565), 1515–1532.
Hoinka, K.P., 1998. Statistics of the global tropopause pressure. Mon. Weather Rev. 126 (12), 3303–3325.
Hoinka, K.P., 1999. Temperature, humidity, and wind at the global tropopause. Mon. Weather Rev. 127 (10), 2248–2265.
Holton, J.R., Haynes, P.H., Mclntyre, M.E., Douglass, A.R., Rood, R.B., Pfister, L., 1995. Stratosphere-troposphere exchange. Rev. Geophys. 33 (4), 403–439.
Kishore, P., Namboothiri, S.P., Igarashi, K., Jiang, J.H., Ao, C.O., Romans, L.J., 2006. Climatological characteristics of the tropopause parameters derived from GPS/CHAMP and GPS/SAC-C measurements. J. Geophys. Res. 111 (D20).
Kuleshov, Y., Choy, S., Fu, E.F., Chane-Ming, F., Liou, Y.-A., Pavelyev, A.G., 2016. Analysis of meteorological variables in the Australasian region using ground- and space-based GPS techniques. Atmos. Res. 176, 276–289.
Kumar, V., Dhaka, S.K., Reddy, K.K., Gupta, A., Prasad, S.B.S., Panwar, V., Singh, N., Ho, S.P., Takahashi, M., 2014. Impact of quasi-biennial oscillation on the inter-annual variability of the tropopause height and temperature in the tropics: a study using COSMIC/FORMOSAT-3 observations. Atmos. Res. 139, 62–70.
Kuo, Y.H., Wee, T.K., Sokolovskiy, S., Rocken, C., Schreiner, W., Hunt, D., Anthes, R.A., 2004. Inversion and error estimation of GPS radio occultation data. J. Meteorol. Soc. Jpn. 82 (1B), 507–531.
Kuo, Y.H., Schreiner, W.S., Wang, J., Rossiter, D.L., Zhang, Y., 2005. Comparison of GPS radio occultation soundings with radiosondes. Geophys. Res. Lett. 32 (5).
Liou, Y.A., Pavelyev, A.G., 2006. Simultaneous observations of radio wave phase and intensity variations for locating the plasma layers in the ionosphere. Geophys. Res. Lett. 33 (L23102). http://dx.doi.org/10.1029/2006GL027112.
Liou, Y.A., Pavelyev, A.G., Wickert, J., Schmidt, T., Pavelyev, A.A., 2005. Analysis of atmospheric and ionospheric structures using the GPS/MET and CHAMP radio occultation database: a methodological review. GPS Solutions 9 (2):122–143. http://dx.doi.org/10.1007/s10291-005-0141-y.
Liou, Y.A., Pavelyev, A.G., Liu, S.F., Pavelyev, A.A., Yen, N., Huang, C.Y., Fong, C.J., 2007. FORMOSAT-3/COSMIC GPS radio occultation mission: preliminary results. IEEE Trans. Geosci. Remote Sens. 45 (11), 3813–3826.
Liou, Y.A., Pavelyev, A.G., Matyugov, S.S., Yakovlev, O.I., Wickert, J., 2010. Radio occultation method for remote sensing of the atmosphere and ionosphere. In: Liou, Y.A. (Ed.), Radio Occultation Method for Remote Sensing of the Atmosphere and Ionosphere. InTech.
Nishida, M., Shimizu, A., Tsuda, T., Rocken, C., Ware, R.H., 2000. Seasonal and longitudinal variations in the tropical tropopause observed with the GPS occultation technique (GPS/MET). J. Meteorol. Soc. Jpn. 78 (6), 691–700.
Randel, W.J., Wu, F., Ríos, W.R., 2003. Thermal variability of the tropical tropopause region derived from GPS/MET observations. J. Geophys. Res. 108 (D1).
Reid, G.C., Gage, K.S., 1996. The tropical tropopause over the western Pacific: wave driving, convection, and the annual cycle. J. Geophys. Res. 101 (D16), 21,233–21,241.
Santer, B.D., Sausen, R., Wigley, T.M.L., Boyle, J.S., Achuta, R.K., Doutriaux, C., Hansen, J.E., Meehl, G.A., Roeckner, E., Ruedy, R., Schmidt, G., Taylor, K.E., 2003a. Behavior of tropopause height and atmospheric temperature in models, reanalyses, and observations: decadal changes. J. Geophys. Res. 108 (D1).
Santer, B.D., Wehner, M.F., Wigley, T.M.L., Sausen, R., Meehl, G.A., Taylor, K.E., Ammann, C., Arblaster, J., Washington, W.M., Boyle, J.S., Brüggemann, W., 2003b. Contributions of anthropogenic and natural forcing to recent tropopause height changes. Science 301 (5632), 479–483.
Santhi, Y.D., Ratnam, M.V., Dhaka, S.K., Rao, S.V., 2014. Global morphology of convection indices observed using COSMIC GPS RO satellite measurements. Atmos. Res. 137, 205–215.
Sausen, R., Santer, B.D., 2003. Use of changes in tropopause height to detect human influences on climate. Meteorol. Z. 12 (3), 131–136.
Schmidt, T., Wickert, J., Beyerle, G., Reigber, C., 2004. Tropical tropopause parameters derived from GPS radio occultation measurements with CHAMP. J. Geophys. Res. 109 (D13).
Schmidt, T., Heise, S., Wickert, J., Beyerle, G., Reigber, C., 2005. GPS radio occultation with CHAMP and SAC-C: global monitoring of thermal tropopause parameters. Atmos. Chem. Phys. 5, 1473–1488.
Schmidt, T., Wickert, J., Beyerle, G., Heise, S., 2008a. Global tropopause height trends estimated from GPS radio occultation data. Geophys. Res. Lett. 35 (11).
Schmidt, T., Wickert, J., Heise, S., Flechtner, F., Fagiolini, E., Schwarz, G., Zenner, L., Gruber, T., 2008b. Comparison of ECMWF analyses with GPS radio occultations from CHAMP. Ann. Geophys. 26 (11), 3225–3234.
Schreiner, B., Hunt, D., Rocken, C., Sokolovskiy, S., 2003. Radio occultation data processing at the COSMIC Data Analysis and Archival Center (CDAAC). In: Reigber, C., Lühr, H., Schwintzer, P. (Eds.), First CHAMP Mission Results for Gravity, Magnetic and Atmospheric Studies. Springer Berlin, Heidelberg, pp. 536–544.
Schreiner, W., Rocken, C., Sokolovskiy, S., Syndergaard, S., Hunt, D., 2007. Estimates of the precision of GPS radio occultations from the COSMIC/FORMOSAT-3 mission. Geophys. Res. Lett. 34 (4).
Schreiner, W., Sokolovskiy, S., Hunt, D., Rocken, C., Kuo, Y.H., 2011. Analysis of GPS radio occultation data from the FORMOSAT-3/COSMIC and Metop/GRAS missions at CDAAC. Atmos. Meas. Tech. 4 (10), 2255–2272.
Seidel, D.J., Randel, W.J., 2006. Variability and trends in the global tropopause estimated from radiosonde data. J. Geophys. Res. 111 (D21).
Seidel, D.J., Ross, R.J., Angell, J.K., Reid, G.C., 2001. Climatological characteristics of the tropical tropopause as revealed by radiosondes. J. Geophys. Res. 106 (D8), 7857–7878.
Shepherd, T.G., 2002. Issues in stratosphere-troposphere coupling. J. Meteorol. Soc. Jpn. 80 (4B), 769–792.
Sokolovskiy, S., Rocken, C., Hunt, D., Schreiner, W., Johnson, J., Masters, D., Esterhuizen, S., 2006. GPS profiling of the lower troposphere from space: inversion and demodulation of the open-loop radio occultation signals. Geophys. Res. Lett. 33 (14).
Son, S.W., Tandon, N.F., Polvani, L.M., 2011. The fine-scale structure of the global tropopause derived from COSMIC GPS radio occultation measurements. J. Geophys. Res. 116 (D20).
Sun, B.M., Reale, A., Seidel, D.J., Hunt, D.C., 2010. Comparing radiosonde and COSMIC atmospheric profile data to quantify differences among radiosonde types and the effects of imperfect collocation on comparison statistics. J. Geophys. Res. 115 (D23).
Wang, B.-R., Liu, X.-Y., Wang, J.-K., 2013. Assessment of COSMIC radio occultation retrieval product using global radiosonde data. Atmos. Meas. Tech. 6 (4), 1073–1083.
Wickert, J., Reigber, C., Beyerle, G., König, R., Marquardt, C., Schmidt, T., Grunwaldt, L., Galas, R., Meehan, T.K., Melbourne, W.G., Hocke, K., 2001. Atmosphere sounding by GPS radio occultation: first results from CHAMP. Geophys. Res. Lett. 28 (17), 3263–3266.
Wickert, J., Schmidt, T., Beyerle, G., König, R., Reigber, C., 2004a. The radio occultation experiment aboard CHAMP: operational data analysis and validation of vertical atmospheric profiles. J. Meteorol. Soc. Jpn. 82 (1B), 381–395.
Wickert, J., Pavelyev, A.G., Liou, Y.-A., Schmidt, T., Reigber, C., Igarashi, K., Pavelyev, A.A., Matyugov, S., 2004b. Amplitude variations in GPS signals as a possible indicator of the ionospheric structures. Geophys. Res. Lett. 31 (L24801). http://dx.doi.org/10.1029/2004GL020607.
Wickert, J., Beyerle, G., König, R., Heise, S., Grunwaldt, L., Michalak, G., Reigber, C., Schmidt, T., 2005. GPS radio occultation with CHAMP and GRACE: a first look at a new and promising satellite configuration for global atmospheric sounding. Ann. Geophys. 23 (3), 653–658.
Wickert, J., Arras, C., Ao, C.O., Beyerle, G., Falck, C., Grunwaldt, L., Healy, S.B., Heise, S., Helm, A., Huang, C.Y., Jakowski, N., König, R., Mannucci, T., Mayer, C., Michalak, G., Rothacher, M., Schmidt, T., Stosius, R., Tapley, B., 2008. CHAMP, GRACE, SAC-C, TerraSAR-X/Tandem-X: science results, status and future prospects. GRAS SAF Workshop on Applications of GPSRO Measurements, Reading, UK, 16–18 June 2008.
Wickert, J., Michalak, G., Schmidt, T., Beyerle, G., Cheng, C.-Z., Healy, S.B., Heise, S., Huang, C.-Y., Jakowski, N., Köhler, W., Mayer, C., Offiler, D., Ozawa, E., Pavelyev, A.G., Rothacher, M., Tapley, B., Arras, C., 2009a. GPS radio occultation: results from CHAMP, GRACE and FORMOSAT-3/COSMIC. Terr. Atmos. Ocean. Sci. 20 (1), 35–50.
Wickert, J., Schmidt, T., Michalak, G., Heise, S., Arras, C., Beyerle, G., Falck, C., Konig, R., Pingel, D., Rothacher, M., 2009b. GPS radio occultation with CHAMP, GRACE-A, SAC-C, TerraSAR-X, and FORMOSAT-3/COSMIC: brief review of results from GFZ. In: Steiner, A., Pirscher, B., Foelsche, U., Kirchengast, G. (Eds.), New Horizons in Occultation Research. Springer, Berlin Heidelberg, pp. 3–15.
World Meteorological Organization, 1957. Definition of the tropopause. WMO Bull. 6 (Geneva, Switzerland).
Xu, X., Luo, J., Shi, C., 2009. Comparison of COSMIC radio occultation refractivity profiles with radiosonde measurements. Adv. Atmos. Sci. 26 (6), 1137–1145.
Zängl, G., Hoinka, K.P., 2001. The tropopause in the polar regions. J. Clim. 14 (14), 3117–3139.
Zhang, K., Fu, E., Silcock, D., Wang, Y., Kuleshov, Y., 2011. An investigation of atmospheric temperature profiles in the Australian region using collocated GPS radio occultation and radiosonde data. Atmos. Meas. Tech. 4 (10), 2087–2092.